Influence of Abrasive Water Jet parameters on the surface integrity of Inconel 718

Lorena Cano Salinas
Institut Clément Ader
Kamel Moussaoui
Institut Clément Ader
Akshay Hejjaji
Institut Clément Ader
Mehdi Salem
Institut Clément Ader
Anis Hor
Institut Clément Ader
Redouane Zitoune (redouane.zitoune@iut-tlse3.fr)
Institut Clèment Ader https://orcid.org/0000-0003-4375-0998

Research Article

Keywords: AWJ, Inconel 718, Roughness, Topography, Depth of cut, Residual stresses

Posted Date: March 18th, 2021

DOI: https://doi.org/10.21203/rs.3.rs-197952/v1

Version of Record: A version of this preprint was published at The International Journal of Advanced Manufacturing Technology on March 25th, 2021. See the published version at https://doi.org/10.1007/s00170-021-06888-9.

Influence of Abrasive Water Jet parameters on the surface integrity of Inconel 718

Lorena Cano Salinas[a], Kamel Moussaoui[a], Akshay Hejjaji[a], Mehdi. Salem[b], Anis Hor[a], Redouane Zitoune[a*]

[a] Institut Clément Ader, CNRS UMR 5312, 3 Rue Caroline Aigle, 31400 Toulouse, France
[b] Institut Clément Ader, CNRS UMR 5312, Campus Jarlard, 81013 Albi
*Corresponding authors: redouane.zitoune@iut-tlse3.fr

Abstract

Inconel 718 (IN718) is a precipitation hardened nickel-base super-alloy exhibiting high strength and good corrosion resistance at elevated temperatures and on the downside it is characterized by poor machinability. Abrasive Water Jet (AWJ) process, offers a potential method to machining difficult-to-cut materials such as IN718. The present work investigates the influence of Abrasive Water Jet parameters on surface roughness, topography, depth of cut and residual stress when milling IN718. Surface characterization was conducted through 3D optical microscopy and SEM techniques. Residual stresses were measured in longitudinal and transverse directions with respect to the machining path using X-ray diffraction (XRD) technique. The obtained results showed that milled surfaces have a homogeneous texture with embedded abrasive particles and high surface roughness. AWJ process introduced high compressive residual stresses with similar order of level in both directions (X and Y). In addition, it was observed that jet pressure is the most influencing parameter on roughness and depth of cut, whilst traverse speed and step-over distance had a significant effect on the residual stress. Based on the experimental analysis, an empirical model to predict the depth of cut was proposed. The validation of the proposed model, has shown around 5% error in the predicted and actual pocket depth.

Keywords: AWJ, Inconel 718, Roughness, Topography, Depth of cut, Residual stresses

1 Introduction

Nickel-based super alloys are widely used for aircraft engines, gas turbines and in industries like petrochemical and oil refineries. Inconel 718 (IN718) is a precipitation hardened nickel-based super-alloy. The most important properties of IN718 are high strength at elevated temperatures, good corrosion resistance and high hardness [1, 2]. The retention of its properties during machining combined with its poor thermal conductivity makes Inconel 718 difficult to machine by conventional machining processes [1].

Several studies dealing with the influence of conventional machining on surface integrity of IN718 reports problems caused by the interaction of the cutting tool and the target material due to the mechanical and thermal loads during machining. These problems include an excessive and rapid tool wear which results in a poor surface quality in form of defects as built-up edges (BUE), tears, cavities, burrs, etc. [3, 4, 5]. Other difficulties reported are a distortion in the microstructure of IN718 which could be plastic deformation or recrystallization leading to grain refinement and changes in morphology and orientation of the grain [3, 5, 6, 7, 8]. Regarding mechanical state, the investigations report a tensile residual stress state at the surface which then shifts to compressive residual state beneath the surface [9, 6, 3, 5]. For a finish-machined surface, a tensile residual stress has a detrimental impact from a fatigue loading perspective where it is preferred to have a compressive residual stress state [6]. In order to reduce these topographical, metallurgical and mechanical alterations of the target material after conventional machining, studies have used lubrication [4, 5, 10], however, this practice is not always effective and has a negative environmental impact. In fact, Abrasive Water Jet (AWJ) machining process provides an alternative to mitigate difficulty in IN718 machining. AWJ seems to be more relevant than conventional process from the point of view of microstructure because of conventional machining induces higher and deeper strain-hardening and damage than AWJ [6]. AWJ is a non-conventional machining process, which uses high-pressure water forced through a nozzle and mixed with abrasive grit particles and directed towards a workpiece as a high-velocity jet focused to erode a desired material. Originally AWJ was developed for through cutting operations of difficult-to-cut materials by conventional machining processes; whilst AWJ for milling process (controlled-depth) has been less developed [11, 12, 13]. The main advantages of AWJ machining are minimized heat affected zone on the workpiece and the versatility to cut any kind of materials from soft to very hard, such as titanium or Inconel [14, 15].

AWJ is characterized by a large number of process parameters [16], $viz.$ jet pressure, traverse speed, abrasive flow rate, abrasive grit size, stand-off distance, step-over distance, nozzle diameter, orifice diameter and length of the focusing tube. These parameters influenced the characteristics of the machined surface, for example, in in the work conducted by [17, 18], when machining stainless steel, authors proved that the impact of abrasive flow rate as well as the vibration phenomenon that occur during the cutting

process affect the machining quality. It was clearly noticed that the poor machining quality occurs when machining is conducted at high transverse speed and at higher absolute values of material vibrations [18]. In addition, if we refer to the work of [14], it was shown that the most influential parameters on the surface topography and microstructural or mechanical characteristics are jet pressure, traverse speed, stand-off distance and abrasive flow rate. In addition, in the works conducted by Flower et. al and Gupta et. al [13,14] it was shown that the increase in abrasive particle size favors the increase in the material removal rate, however, it leads to degradation of machining quality giving a very poor surface roughness. In fact, to counter this problem, the works conducted by Xavier et al. and Hejjaji et al. [19, 20] recommend a medium mesh size of (#120) abrasive particles to strike a balance between surface quality and material removal rate.

The availability of literature on the influence of the AWJM parameters on the surface characteristics after machining IN718 is limited. The investigation by Bhandarkar et al. [21] focuses on characterizing pockets milled by AWJ in order to optimize process parameters for pocket dimensions and the average surface roughness (Ra). In their work, it was mentioned that the optimal machining parameters to achieve the requested geometry of the depth pocket were a jet pressure of $140\ MPa$ and transverse speed of $1\ m/min$. In addition, it was mentioned that the average roughness of the machined surface decreases when machining is conducted at lower pressure and at higher traverse speed. In the experimental work conducted by Rivero et al. [22], it was shown that the direction of milling (tool path) does not have any effect on the surface roughness. It was also reported by the same authors that the main parameters responsible of the surface roughness are the jet pressure, the abrasive flow rate and the stand-off distance. However, the stand-off distance showed a more impact on the roughness values compared to the jet pressure and the transverse speed. In fact, it was shown that, machining with a stand-off distance of $10\ mm$ allowed to obtain a small roughness and less embedded particles on the machined surface compared to the case of machining with high stand-off distance. Unfortunately, milling with a small stand of distance ($10\ mm$) cannot be possible when workpiece has complex features like concave/convex curvature. In this case of machining advanced tool compensation needs to programmed, to avoid this issue, Cenac et al. [23] recommend using of stand-off distance of $100\ mm$ when machining fuselage parts of aircrafts.

Holmberg et al. [6] studied a comparison of the machinability of Inconel alloy 718 during milling with different processes: conventional milling, Electron Discharge Machining (EDM), laser and AWJ. The comparison has been performed with only one milling condition for each machining process. Indeed, for AWJ they used a pressure of $380\ MPa$ and $0.11\ m/min$ of traverse speed, that produced highly desirable surface with low surface roughness ($Sa = 1.8\ \mu m$) and high compressive residual stress up to $-700\ MPa$ at the surface. However, no information is available about the influence of the parameters of AWJ process on the residual stress when machining Inconel. In another work, Escobar-Palafox et al. [24] investigated pocket milling of IN718 in terms of geometry and depth of cut when using different process parameters,

including low pressures below $105\ MPa$, traverse speed between 0.016 and $0.08\ m/min$ and step-over distance from 0.5 to $0.8\ mm$. They showed that the jet pressure is the main parameter influencing the depth of cut. However, the influence of the jet pressure on the depth of cut exhibits non-linear behavior. Further, when lower traverse speed is used, higher abrasive flow rate is required to achieve deeper depth of cut. Unfortunately, using higher abrasive flowrate favors the augmentation of the surface roughness [13, 14]. In fact, this phenomenon can be explained by the fact that when machining is conducted with small transverse speed the kinetic energy carried by the particles to the work piece is higher than the case of machining with high transverse speed. Similar results have been obtained by Ay et al. [25] during their investigation on the effect of traverse speed on kerf shape by cutting a single slot. In fact, it was concluded that lower traverse speed generates deeper depth of cut and wider kerf because at lower traverse speeds more time is needed for cutting, leading to increased jet overlapping on the target material.

The present work focuses on the influence of the AWJ process parameters on the roughness, surface topographical characteristics, depth of cut and residual stresses during milling of IN718. For this, a full factorial experiment with 3 factors ($viz.$ water jet pressure, traverse speed and step-over distance) at 3 levels was adopted for investigation. After machining, the roughness, depth of cut and residual stresses of the specimens have been measured and characterized as a function of the machining parameters. In addition, an empirical model is proposed for the prediction of the depth of cut, which is based on the total pocket depth.

2 Experimental procedure

The material used is this study was annealed Inconel alloy 718 with an ultimate tensile strength of $903\ MPa$, a yield strength of $450\ MPa$, and an elongation of 50%. The chemical content of the material is given in **Table 1**. Full factorial experiments were performed on specimens of size $180\ mm\ x\ 20\ mm\ x\ 3.71\ mm$ on an Abrasive Water Jet Machine Flow MACH4-C. The details of some major machine components are as follows, orifice diameter of $0.33\ mm$, a focusing tube length of $76\ mm$ and nozzle diameter of $1.016\ mm$. Also, abrasive garnet of mesh size $\#120$ is used in the present work. As mentioned in the introduction, machining with the mesh size of #120 favors an acceptable surface roughness without compromising in material removal rate (machining time). **Fig. 1** shows the experimental setup for milling by AWJ. All experiments are carried out keeping a constant stand-off distance and abrasive flow rate. Each test sample was milled in order to create four blind pockets of $20\ mm$ of length each spaced $20\ mm$ following a raster scan tool path (**Fig. 2**a) and keeping jet direction changes outside the workpiece to avoid acceleration and deceleration effects on milling. Jet pressure, traverse speed and step-over distance parameters were varied at three different levels in order to accomplish a total

experimental design of 27 experiments. The process parameters used to perform the machining are specified in **Table 2**. Each experiment was repeated for four times by creating four pockets with same set of machining parameters (**Fig. 2**b) in order to ensure good reliability of the process.

Table 1 Chemical composition of the investigated Inconel 718 specimens

Ni (%)	Cr (%)	Fe (%)	Nb (%)	Mo (%)	Ti (%)	Al (%)	Co (%)	C (%)	Mn (%)	Si (%)	S (%)	P (%)	B (%)	Cu (%)	Ta (%)
53.47	18.28	18.2	5.06	2.98	0.96	0.51	0.17	0.03	0.09	0.08	0.0003	0.007	0.001	0.06	0.01

Fig. 1. Experimental setup for AWJ milling.

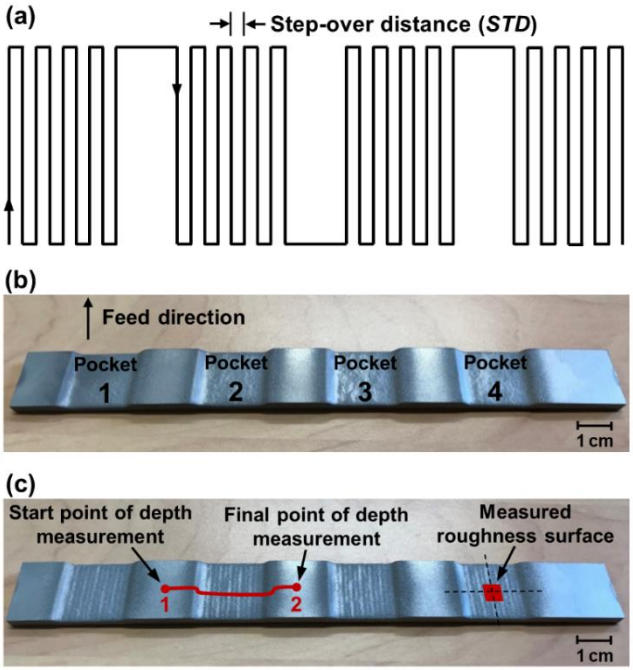

Fig. 2. (a) Tool path; (b) Sample machined at $P = 250\ MPa$, $f = 1\ m/min$ and $STD = 0.5\ mm$; (c) Location of pocket depth and roughness measurements of the pocket 2 and the pocket 4 respectively of the specimen milled at $P = 300\ MPa$, $f = 0.5\ m/min$ and $STD = 1.5\ mm$.

Table 2 AWJ milling parameters

Parameter	Setting	Unit
Pressure (P)	200, 250, 300	MPa
Traverse speed (f)	0.5, 1, 1.5	m/min
Step-over distance (STD)	0.5, 1, 1.5	mm
Stand-off distance	100	mm
Abrasive flow rate	0.18	kg/min

The characterization of the machined surface was done in terms of surface roughness, pocket depth and residual stress. The roughness measurements of all pockets were performed using an Alicona Infinite Focus 3D optical profilometer over a surface area of $5.7\ mm\ x\ 5.7\ mm$ at the center of each machined pocket (**Fig. 2**c) with a vertical and lateral resolution of $0.10\ \mu m$ and $4.00\ \mu m$ respectively. In order to correctly treat the measured data, three steps were performed before the surface roughness analysis. First, the data set was treated for leveling to remove measurement errors due to parallelism problem between profilometer sensor and the target sample. Then, the unmeasured points of the scanned surfaces were filled by interpolation method. Finally, the scanned surfaces were cropped to a size of $5\ x\ 5\ mm$ in order to remove measurement errors due to edge effects. No filter was applied for treating the 3D data set.

The pocket depth of each machined pocket was measured using an Altisurf © 520v microscope. The pocket profile was measured by scanning a profile of $40\ mm\ x\ 2\ mm$ in longitudinal direction starting at a point on non-machined surface (1) to a final point outside the milled pocket surface (2) as shown in **Fig. 2**c, using vertical resolution of $0.5\ \mu m$ and a lateral resolution of $10\ \mu m$. In order to avoid errors in depth measurement, the data set was leveled using least plane squares method keeping the measurement starting and ending points as reference. In addition, a Gaussian filter was applied to the measured data in order to remove the outliers.

Residual stress measurements were performed by means of X-ray diffraction (XRD) technique. This method was used to estimate the magnitude of the macro-residual stresses on the middle of the machined pocket. Residual stresses were evaluated along the longitudinal direction of the specimen (σ_{11}) and parallel to feed direction (σ_{22}) (**Fig. 3**b). The XRD measurements were performed using 6-axis XRayBot® apparatus equipped with a goniometer with a pure Si solid state detector (**Fig. 3**a). **Table 3** shows the default analysis parameters for Inconel 718. The spot was passed through a circular hole of $5\ mm$ in diameter without collimator. Residual stresses data were computed by StressDiff® software based on the conventional $\sin^2(\psi)$ method.

Table 3 XRD Inconel 718 settings

Choice of radiation source	Mn
Filter	Cr
Fluorescence	/
Diffraction peak	{311}
Voltage	20 kV
Current	1 mA
$2\theta_0$	150°
Acquisition time	120s
Angle of incidence ψ	19

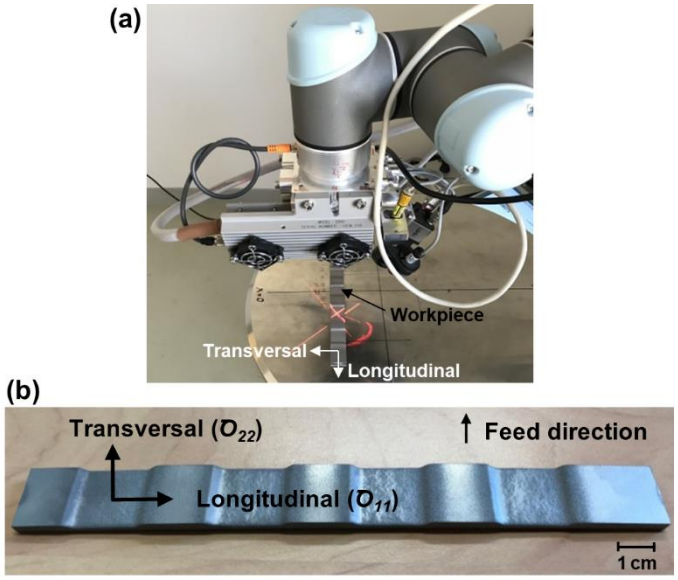

Fig. 3. (a) Setup for the residual stress measurements; (b) Residual stress measurement directions.

3 Results

The results of pocket depth, roughness and residual stress is the average obtained from the measurements made on four pockets with same machining parameters. The specimens $T10$ and $T19$ were not considered for the analysis as the specimens were destroyed upon milling, as the milled depth was higher than the thickness of the workpiece ($3.71\ mm$).

3.1 Surface roughness and topography

Fig. 4 and **Fig. 5** show experimental results in terms of machining parameters and average surface roughness (Sa). The roughness parameter (Sa), is typically used to evaluate surface roughness of an area. The results show relatively high roughness compared to roughness that can be obtained when conventional

process is used [3, 6]. In fact, when milling is conducted with conventional cutting tool, the average roughness Sa reported is around 1 μm when machining with new tool and up to 3.9 μm when machining with a worn tool.

The effect of the jet pressure on the surface roughness when varying traverse speed and step-over distance is presented in the **Fig. 4**. The results show that as pressure and step-over distances are increased, the surface roughness also increases. In addition, an increase in pressure with a decrease in traverse speed leads to an increase in surface roughness (**Fig. 4**a). The fact that that roughness increases with increasing pressure is because at higher pressures, the abrasive particles produce deeper indentations as they possess higher kinetic energy, in the target material and consequently rougher surfaces. This effect was also seen by Rivero et al. [22] when milling alloy 718 by AWJ at different conditions of pressure, stand-off distance, abrasive flow rate and traverse speed.

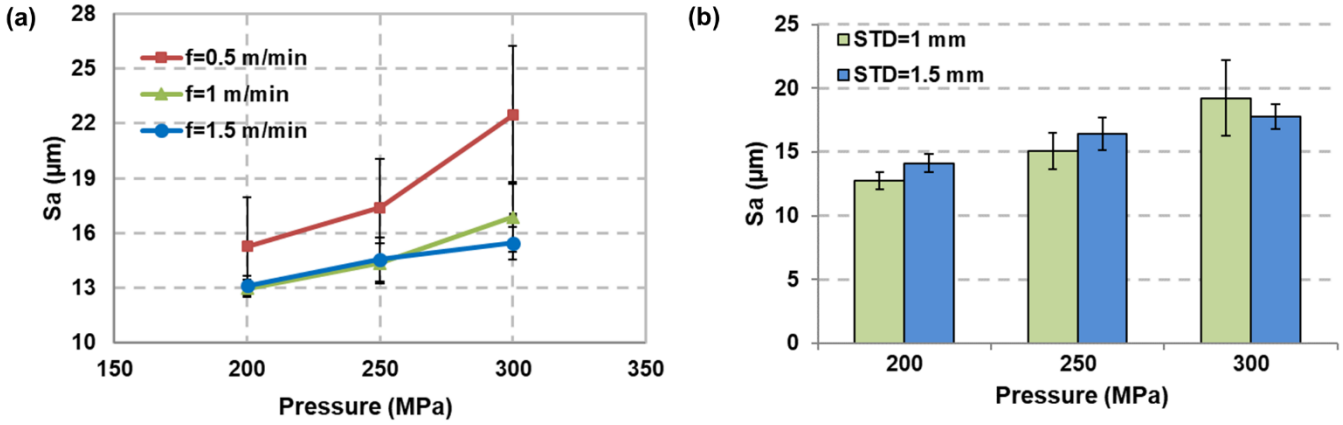

Fig. 4. Effect of the pressure on surface roughness at (a) different traverse speed and (b) different step-over distance.

On the other hand, when the traverse speed increases, the surface roughness tends to decrease (**Fig. 5**). The surface roughness shows a strong decrease when traverse speed increases from 0.5 m/min to 1 m/min. However, the increase of traverse speed beyond 1 m/min the reduction of surface roughness is negligible. This is due to the fact that, the effect of transverse speed on the surface roughness is coupled with the effect of the jet pressure. Hence, for speeds superior to 1 m/min the effect on roughness is less pronounced at low pressures compared to roughness at high pressure (300 MPa), where a clear decreasing effect is seen (**Fig. 5**b). The traverse speeds chosen in this study corresponds to low velocities. In comparison, a study using high traverse speeds ($5 - 15$ m/min), revels no clear effect of traverse speed on surface roughness [22], this investigation states that the size, shape and velocity impact of the abrasive particle is independent to the traverse speed. Conversely, a study performed by Fowler et al. [13] during milling titanium alloys in a single pass using five different abrasives and three different traverse speeds

(1.8, 4.8, 9.96 m/min), observed that a decrease in traverse speed generates lower surface roughness similar to what is seen in this study.

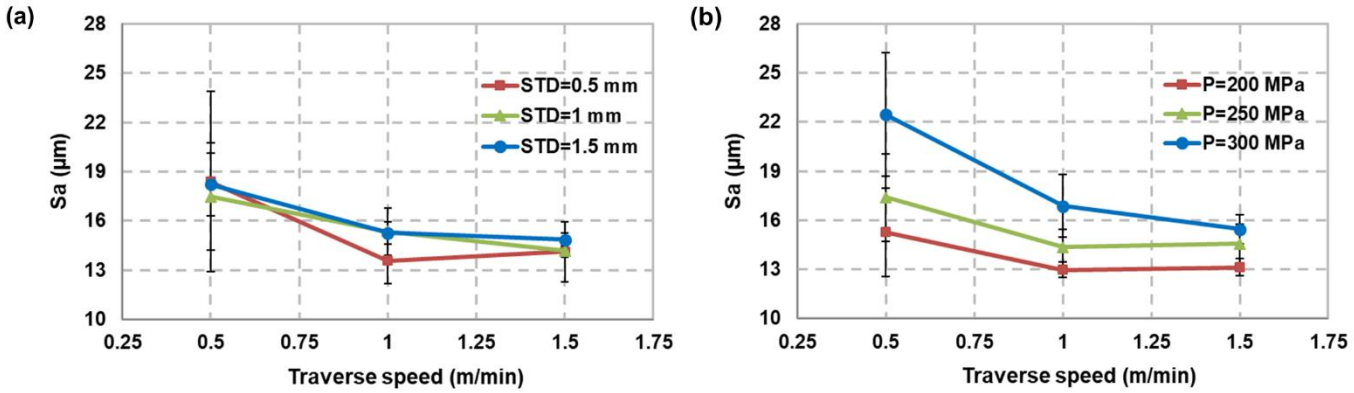

Fig. 5. Mean effect of traverse speed on surface roughness at (a) different step-over distances and (b) at different water pressures.

In the case of STD, there is no clear effect of step-over distance on surface roughness regardless of the jet pressure (**Fig. 6**a). However, it can been seen that surface roughness slightly increases when step-over distance increases for all pressures only at 1.5 m/min of traverse speed (**Fig. 6**b). This increase in surface roughness is a maximum of 1 μm when increasing step-over distance, and up to 3 μm when increasing pressure and step-over distance. Since this increase is slight it could be said that surface roughness remains constant as the pressure and/or step-over distance increase when using traverse speed is 1.5 m/min. For the other two traverse feed rates of 0.5 and 1 m/min there is no clear effect. In any case, it appears that step-over distance parameter have no great impact on surface roughness (**Fig. 6**).

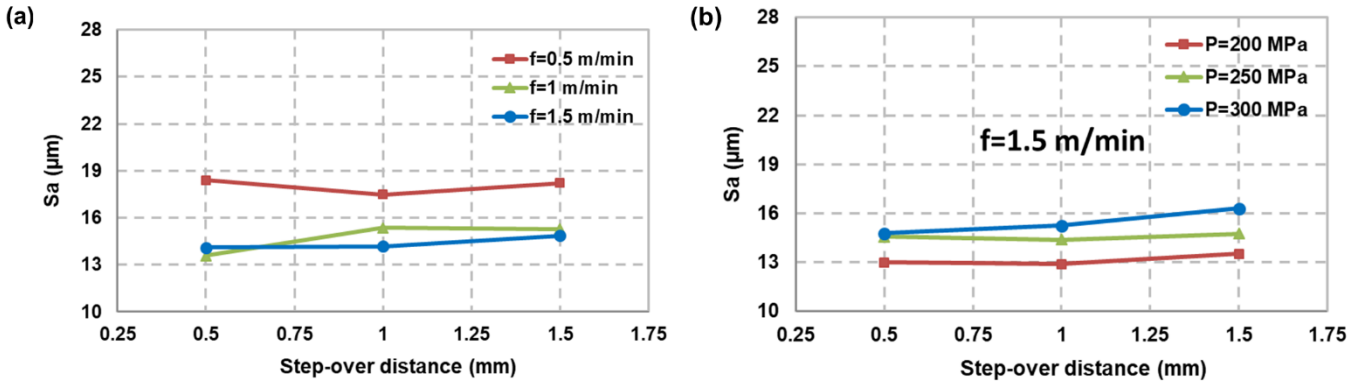

Fig. 6. Effect of step-over distance on surface roughness (a) at different traverse speeds and (b) at different pressures with traverse speed of 1.5 m/min.

The milled surface topographies of some samples are presented in **Fig. 7**, **Fig. 8** and **Fig. 9**. These samples were milled with different AWJ parameters. **Fig. 7** presents the effect of pressure when traverse

speed and step-over distance are constant. It is observed that an increase in pressure leads to an increase in craters (size and depth) which will result in higher roughness. **Fig. 8** shows the effect of three different traverse speeds on surface topography. It is noticed that the effect of increase in traverse speed generates a machined surface with lower surface roughness. In **Fig. 9**, illustrates the effect of step-over distance for a constant traverse speed and pressure. STD does not seem to have a significant effect on the craters and their morphology.

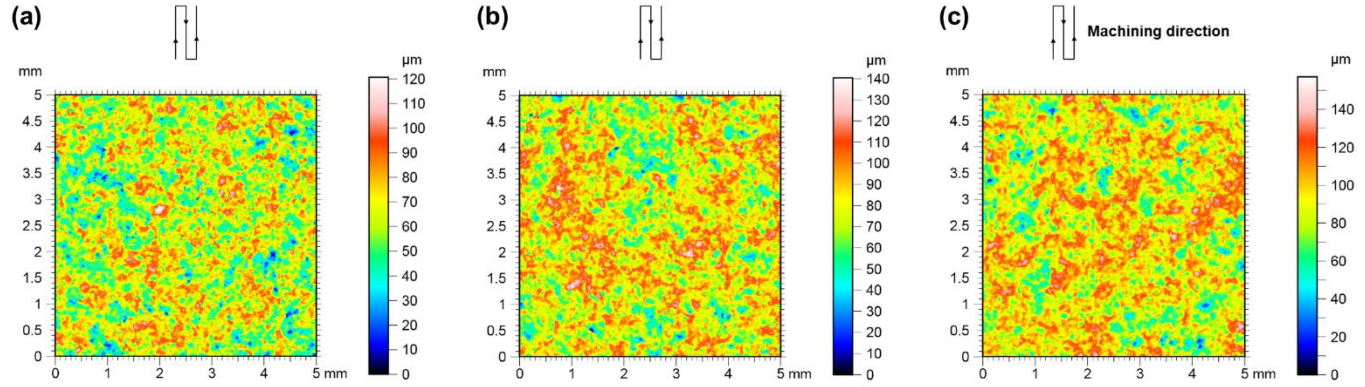

Fig. 7. 3D views of the milled surfaces by AWJ of samples machined at $f = 1.5\ m/min$, $STD = 1\ mm$ and P of (a) $200\ MPa$, (b) $250\ MPa$, and (c) $300\ MPa$.

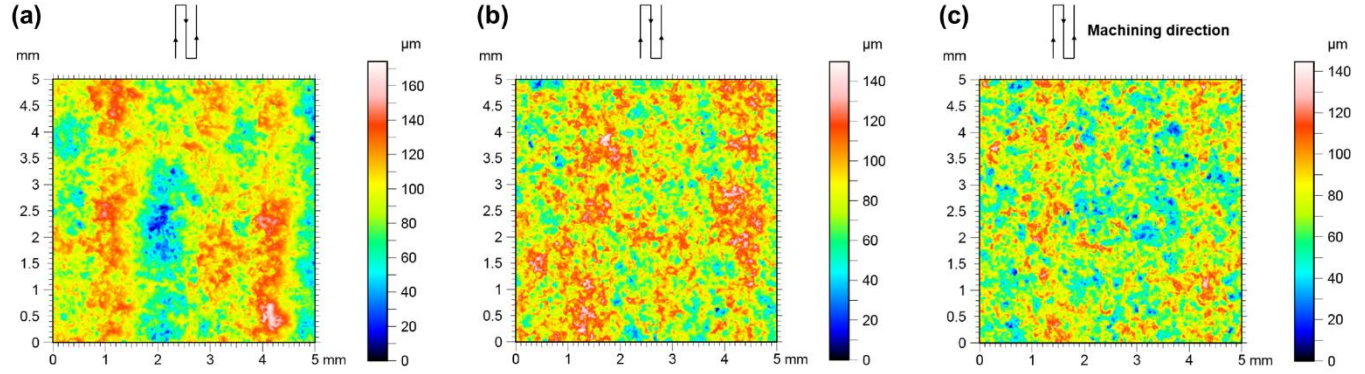

Fig. 8. 3D views of the milled surfaces by AWJ of samples machined at $250\ MPa$ of pressure, $STD = 1.5\ mm$ and (a) $f = 0.5\ m/min$; (b) $f = 1.0\ m/min$ and (c) $f = 1.5\ m/min$.

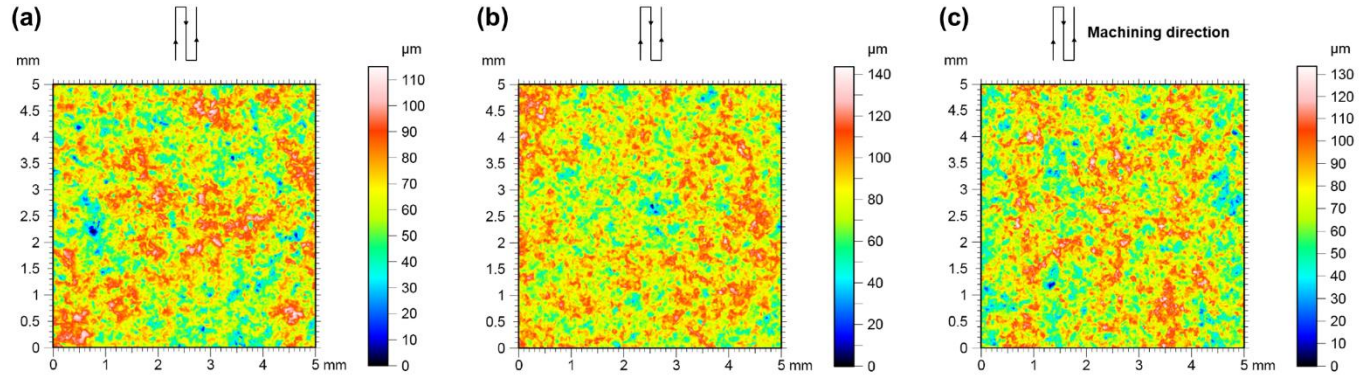

Fig. 9. 3D views of the milled surfaces by AWJ of samples machined at $200\ MPa$ of pressure, $f = 1.5\ m/min$, $P = 200\ MPa$ and (a) $STD = 0.5\ mm$; (b) $STD = 1\ mm$ and (c) $STD = 1.5\ m$.

The different surfaces show a homogeneous texture overall. However, in some machining conditions the milled tracks along the feed direction can be noticed (**Fig. 8**a-b, **Fig. 9**c).

Further analysis of the surface microstructure was performed using SEM at $150x$ magnification in Back Scattered Electron (BSE) mode. **Fig. 10**, **Fig. 11** and **Fig. 12** illustrate the aspect of AWJ milled surfaces at different machining conditions. The images clearly show traces of abrasive particles incrusted during machining. The heavy materials like nickel are identified in bright contrast, light elements like silicon are represented in grey contrast and dark contrast for the organic particles (composed largely of carbon, hydrogen and oxygen). In the micrographs were identified silica (SiO_2) and organic pollutants, which are constituents of the abrasive medium. **Fig. 10** show the microstructure of surfaces milled at different pressures; **Fig. 11** shows images from surfaces machined at different traverse speed; and **Fig. 12** illustrates the micrographs of the surfaces milled using different step-over distances. The surface morphology shows protrusions and valleys on the machined surfaces with plastic deformation due to the impact of the abrasive particles. The presence of these peaks and valleys have detrimental impact on fatigue strength because they favor crack initiation [22]. It is also observed that the material show cased ductile behavior.

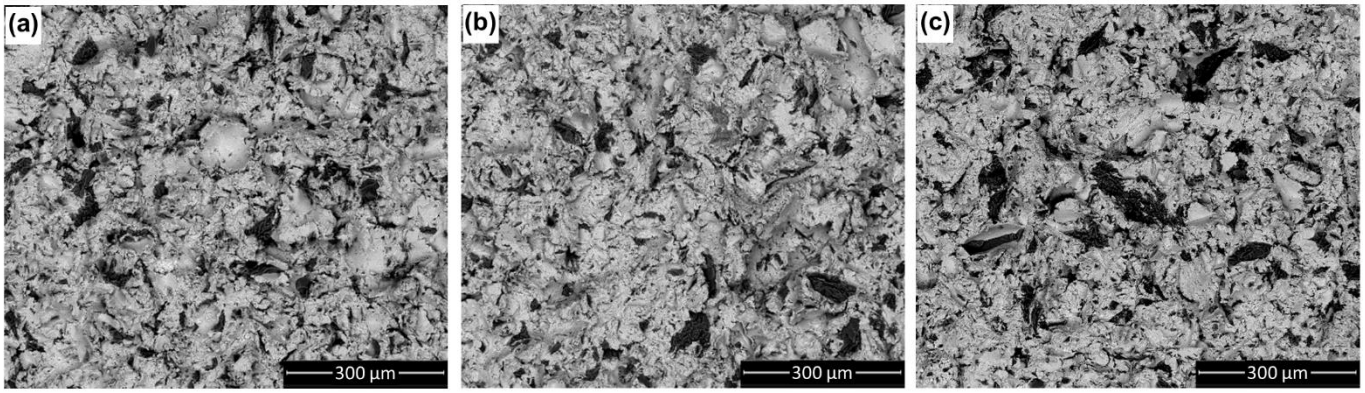

Fig. 10. Micrographs from SEM in x 150 magnification of surfaces machined at $f = 1.5\ m/min$, $STD = 1\ mm$ and P of (a) $200\ MPa$; (b) $250\ MPa$; and (c) $300\ MPa$.

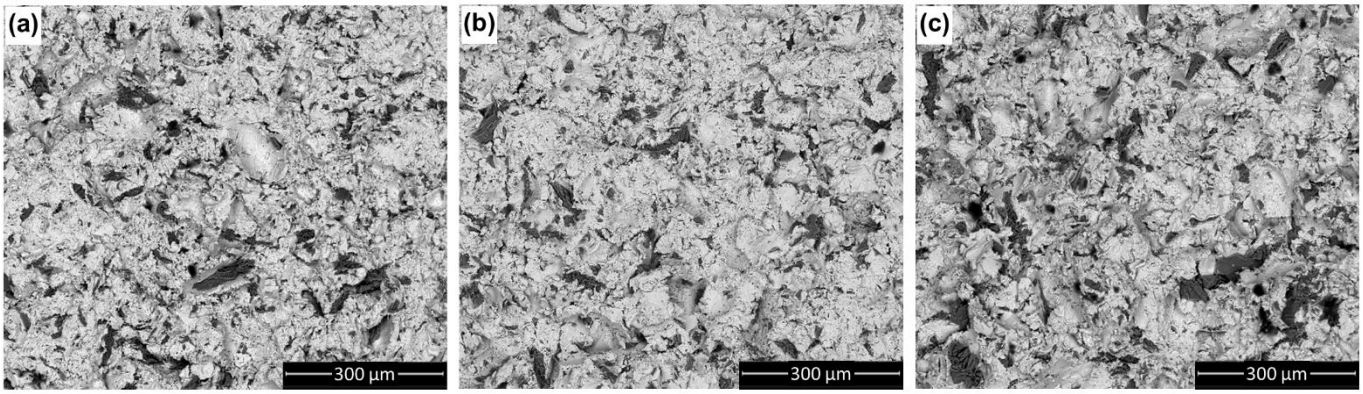

Fig. 11. Micrographs from SEM in x 150 magnification of surfaces machined at 250 MPa of pressure, $STD = 1.5\ mm$ and (a) $f = 0.5\ m/min$; (b) $f = 1.0\ m/min$; and (c) $f = 1.5\ m/min$.

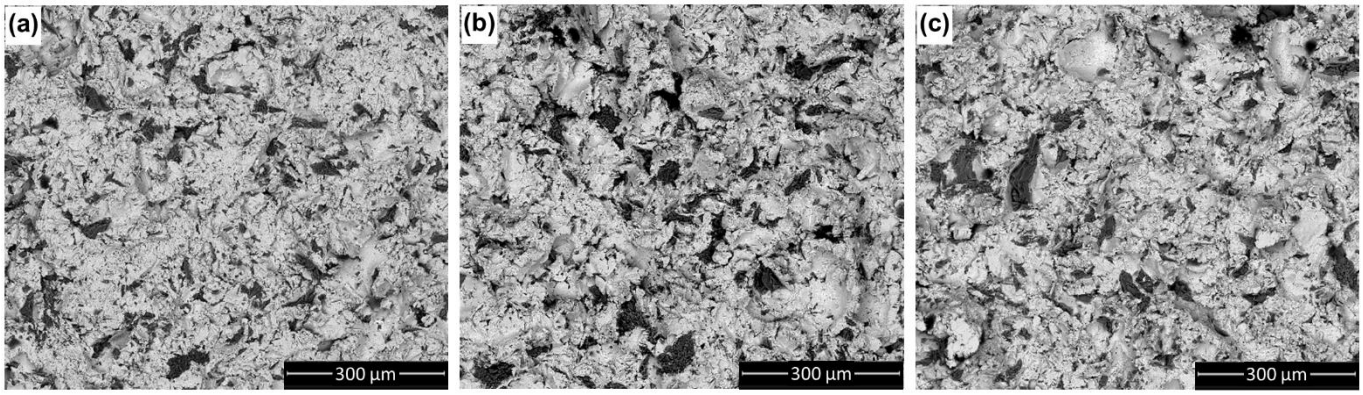

Fig. 12. Micrographs from SEM in x 150 magnification of surfaces machined at 200 $MPa$of pressure, $f = 1.5\ m/min$ and (a) $STD = 0.5\ mm$; (b) $STD = 1\ mm$; and (c) $STD = 1.5\ m$.

Under higher magnification, SEM micrographs show several abrasive particles where large particles are marked with yellow arrows in **Fig. 13** which size can reach about 100 μm in length. In **Fig. 13**a is observed a particle identified as silica in two types of embedment, submerged and incrusted. **Fig. 13**b depicts a dislodgment of material at the crater and several impregnated silica particles, and **Fig. 13**c shows an organic particle.

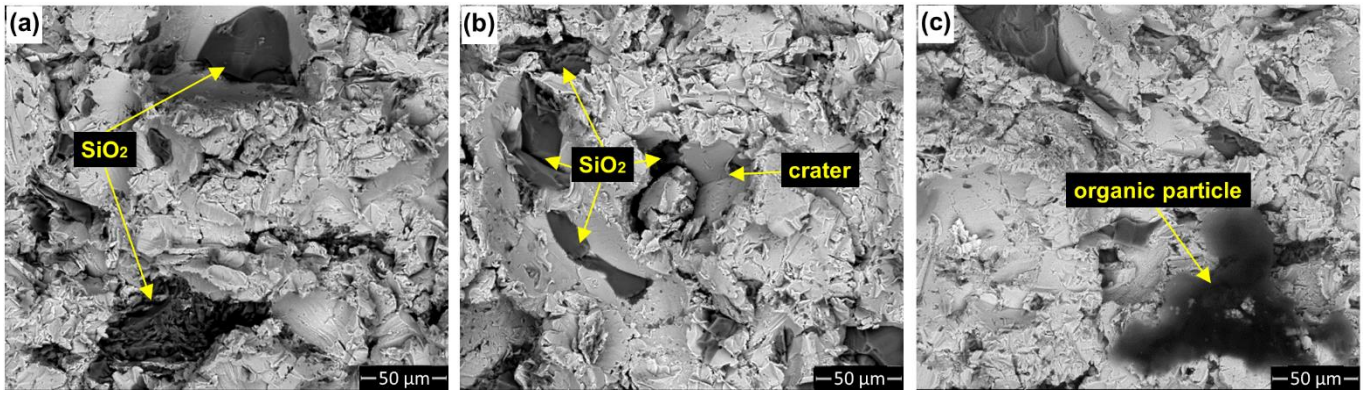

Fig. 13. SEM images of different abrasive particles, (a) silica particles when machining at $P = 200\ MPa$, (b) abrasive particles and crater when machining at $P = 250\ MPa$, and (c) organic particle at when machining at $P = 200\ MPa$.

3.2 Pocket depth

The results summarizing pocket depth with respect to machining parameters are presented in **Table 4**. **Fig. 14** depicts the effect of the pressure, the traverse speed and the step-over distance on the pocket depth. It can be observed that as the pressure is increased, the pocket depth increases (**Fig. 14**a). This can be explained from the fact that the abrasive particles possess high kinetic energy at high pressure and hence high energy transfer occurs between the particle and the target workpiece material leading to removal of more material. On the other hand, for all three pressures considered, the pocket depth decreases when the traverse speed is increased (**Fig. 14**a-c).

Table 4 Variable input parameters and pocket depth output parameters

Exp. No.	P	f	STD	Depth	Std Dev
T1	200	0.5	0.5	2.53	0.09
T2	200	0.5	1	1.22	0.01
T3	200	0.5	1.5	0.80	0.01
T4	200	1	0.5	1.23	0.02
T5	200	1	1	0.59	0.01
T6	200	1	1.5	0.39	0.01
T7	200	1.5	0.5	0.80	0.00
T8	200	1.5	1	0.39	0.01
T9	200	1.5	1.5	0.26	0.01
T10	250	0.5	0.5	-	-
T11	250	0.5	1	1.56	0.02
T12	250	0.5	1.5	1.03	0.02
T13	250	1	0.5	1.58	0.02
T14	250	1	1	0.75	0.01
T15	250	1	1.5	0.49	0.00
T16	250	1.5	0.5	1.01	0.03
T17	250	1.5	1	0.49	0.00
T18	250	1.5	1.5	0.32	0.01
T19	300	0.5	0.5	-	-
T20	300	0.5	1	1.90	0.02
T21	300	0.5	1.5	1.24	0.02
T22	300	1	0.5	1.88	0.05
T23	300	1	1	0.89	0.01
T24	300	1	1.5	0.58	0.00
T25	300	1.5	0.5	1.20	0.01
T26	300	1.5	1	0.57	0.01
T27	300	1.5	1.5	0.38	0.00

P (MPa), f (m/min), STD (mm), Depth (mm)

This effect is due to time of interaction between the water jet and the material surface. Hence, at high traverse speeds the exposure time between water jet and the workpiece surface is reduced leading to reduced amount of energy transfer from the jet to the workpiece material. This results in removal of lesser material and hence lower milling depth. Similar effect was reported by Gupta et al. [14], when performing pocket milling of SS304 specimens using AWJ.

Finally, an increase in the step-over distance leads to a decrease in pocket depth for all the three pressures tested (**Fig. 14**a-c). When using wide step-over distances there is smaller overlapping area between one pass jet and the adjacent, resulting in a lesser amount of material removed.

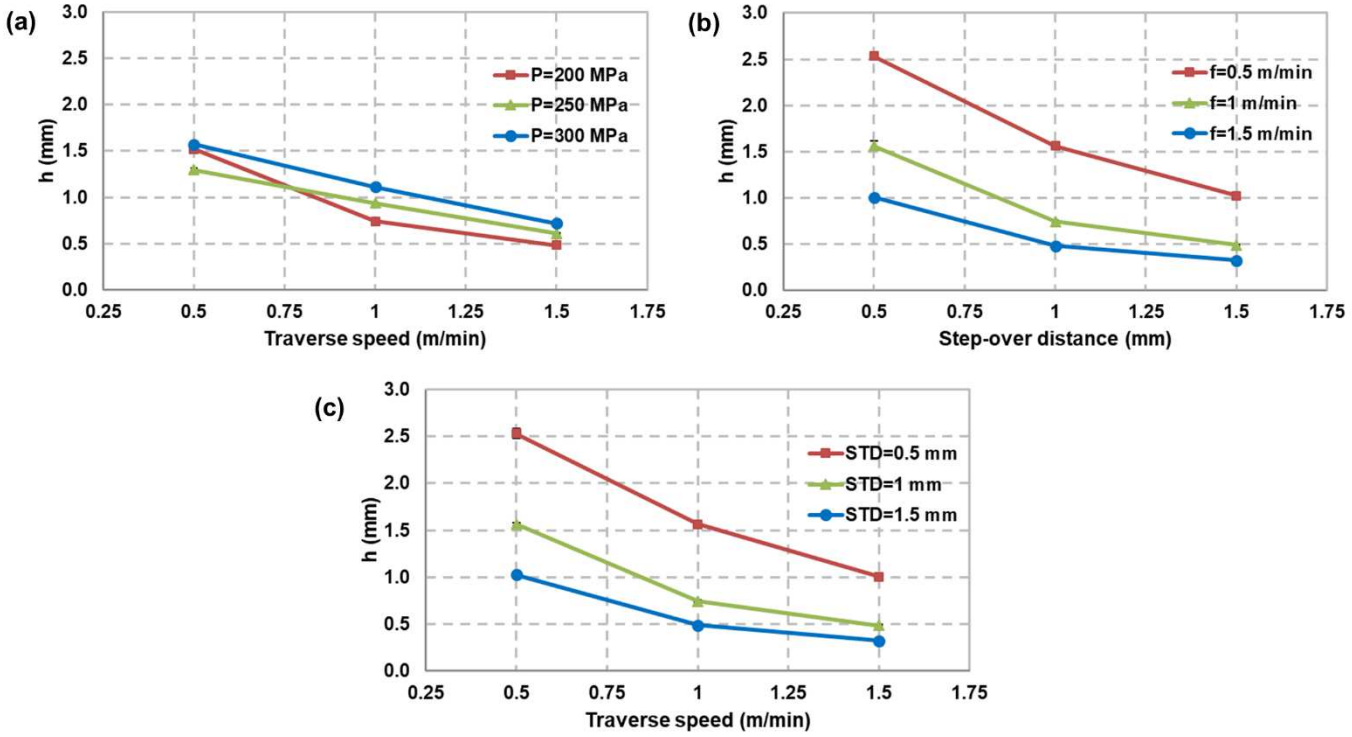

Fig. 14. Effect of the (a) pressure, (b) traverse speed, and (c) step-over distance, on pocket depth.

Furthermore, other interesting parameter is the material removal rate (MRR) to evaluate the efficiency of the AWJM. **Fig. 15** shows that pressure is the parameter that most influences MRR. The increase observed of MRR is of approximately 2.5 mm^3/s each 50 MPa of increase. This phenomenon is due to that at higher pressures, more kinetic energy of the abrasive particles impact on the surface leading to remove more material than at lower pressures. On the other hand, MRR decrease when the traverse speed increases (**Fig. 15**a). This can be explained considering that for greater speeds, the jet collide less time on the surface allowing eliminate shallower layer of material. In respect to step-over distance, it was found that MRR is slightly largest for smaller step-over distances (**Fig. 15**b), this is expected due to smaller step-over distance

allow for a larger overlapping area that leads to remove more material, however, regardless the pressure, when increasing 1 mm in STD the increase in MRR is very low, about 4%.

From the results of pocket depth obtained experimentally, it can be clearly seen that the three parameters of the machining process (pressure, traverse speed and step-over distance) have a great influence on the pocket depth. In this context, the prediction of the pocket in function of the machining parameters is an important requirement for the process to be automated and industrialized.

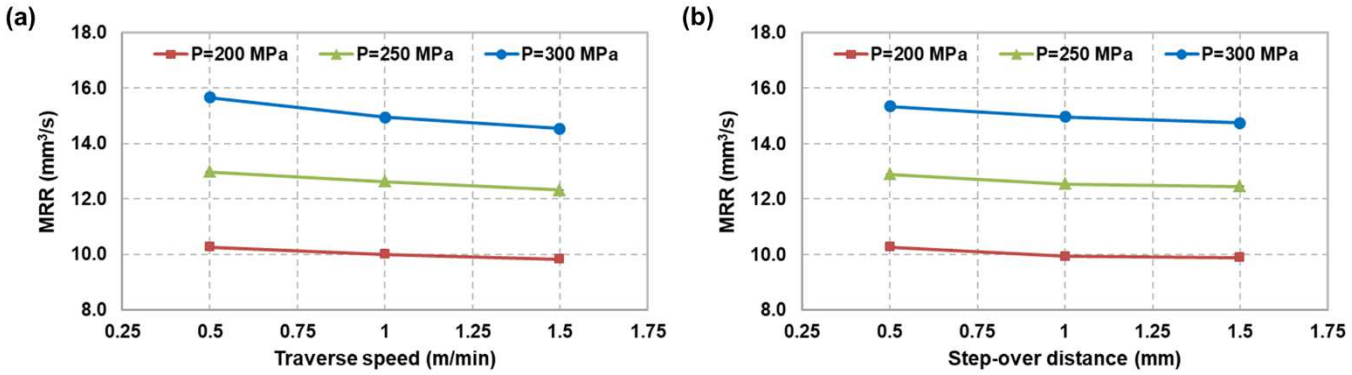

Fig. 15. Effect of (a) the pressure and the traverse speed on the MRR, and (b) the pressure and the step-over distance on the MRR.

3.2.1 Model for the prediction of the depth of cut

Several studies have proposed analytical models for the prediction of the milled pocket depth when machining composite materials and titanium alloys material [26, 27]. In fact, the model proposed here for milling IN718 in function of the process parameters of the AWJ (pressure, traverse speed and step-over distance), is based on the equation (1) from previous literature work [26] related to the machining of composite materials or titanium alloys.

$$H = a \cdot P^b \cdot f^c \cdot S^d \quad (1)$$

Where a, is the constant depending on the machinability of the material. P, f, S represent pressure, traverse speed and step-over distance respectively. In order to feed the model, 22 values of pocket depth from the experimental data set were considered, and the 3 remaining results were set apart for the model validation. The constants a, b, c and d, were identified by a least-squares algorithm. After computing, the resulting constants are presented in equation (2).

$$H = 5.25x10^{-4} \cdot P^{1.306} \cdot f^{-1.057} \cdot S^{-1.052} \quad (2)$$

From the power of coefficients, it can be seen that the jet pressure parameter has the highest influence on the depth of cut, following by traverse speed and step-over distance. This model correlates

well with measured data, as can be seen in **Fig. 16**a, with a coefficient of correlation of 0.9996. Furthermore, the model predicts well the pocket depths, as shown in the comparison between experimental depths and theoretical values (**Fig. 16**b). This model resulted with a maximum uncertainty of 3.9% for $T26$ (which was machined at $P = 300\ MPa$), where the predicted value is overestimated. The second largest difference between experimental and predicted values was of 3.43% for $T9$, the shallowest pocket depth milled at $200\ MPa$. For the deepest pocket $T1$, which was machined at $200\ MPa$, the uncertainty was 0.59%, which is a low variation when high pocket depth is considered. For the specimen set machined at $250\ MPa$, $T18$ presented the mayor relative difference about 1.97%. Moreover, it is noted that for some of the largest differences between predicted and experimental values were for specimens milled at $300\ MPa$.

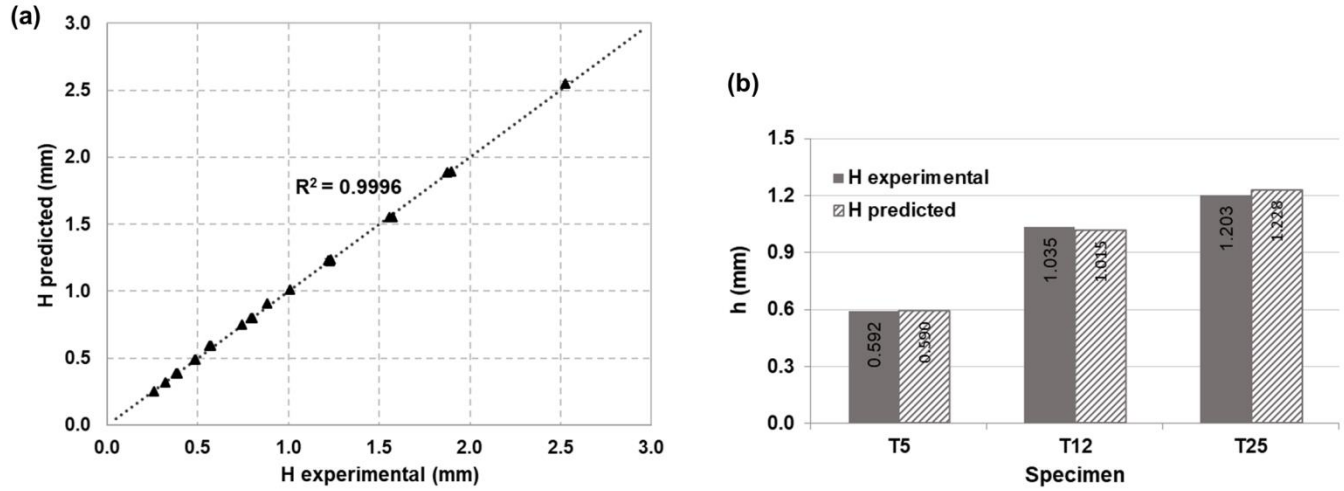

Fig. 16. Graphs of the results of the predicted model, (a) experimental values in function of the predicted ones, and, (b) validation of the model.

Thus, this model fits well with experimental depths of cut, which means that the low difference obtained are mainly due to the material behavior and measurement errors.

3.3 Residual stress

The AWJ milling leads to a compressive residual stress state on the machined surface. The summarized results are presented in **Table 5**. It was observed that both longitudinal and transverse residual stresses are in compression stress state. The longitudinal residual stress varies between $-291.5\ MPa$ and $-648\ MPa$, the transverse residual stress varies between $-297.75\ MPa$ and $-654.75\ MPa$. It can be noted that the values of the longitudinal and transverse residual stresses are very close. This means that the AWJ process does not generate residual stresses in a particular direction unlike conventional machining. This can be explained by the fact that the AWJ process does not favor a direction as for the flow of material

during the material removal in conventional machining. The small difference between longitudinal and traverse residual stress value is due to the effect of the impingement angle of the water jet on the surface owing to the machining direction.

Table 5 Variable input parameters and residual stress output parameters

				Longitudinal			Transverse		
Exp. No.	**P**	**f**	**STD**	**σ_{11}**	**Std Dev**	**Uncertainty**	**σ_{22}**	**Std Dev**	**Uncertainty**
T1	200	0.5	0.5	-533	32.14	55.75	-650.75	18.39	29.25
T2	200	0.5	1	-562.5	9.29	51	-578.5	11.96	34
T3	200	0.5	1.5	-383.5	34.10	56	-364.5	18.48	30.75
T4	200	1	0.5	-515	21.74	52.25	-586	9.06	31.5
T5	200	1	1	-366.75	13.57	54.25	-398.75	8.85	32.25
T6	200	1	1.5	-347.25	13.23	50.5	-384.25	5.38	36.75
T7	200	1.5	0.5	-402.75	10.40	50.75	-429.75	27.44	35.5
T8	200	1.5	1	-326.75	16.28	51.5	-383.25	31.74	28
T9	200	1.5	1.5	-306.5	14.25	53.75	-364	21.97	28.75
T10	250	0.5	0.5	-	-	-	-	-	-
T11	250	0.5	1	-571.25	13.15	50.5	-621	29.68	22.75
T12	250	0.5	1.5	-454.25	35.12	45.25	-462.25	6.65	38.5
T13	250	1	0.5	-638	9.49	44.5	-625	20.18	28.25
T14	250	1	1	-342.5	12.56	46.25	-391.75	12.15	32
T15	250	1	1.5	-309.25	40.82	50.75	-359.75	31.12	23.25
T16	250	1.5	0.5	-407.5	17.94	46.75	-460.25	26.16	25.75
T17	250	1.5	1	-322.75	5.12	50	-351.5	15.02	27.25
T18	250	1.5	1.5	-291.5	24.24	47.75	-297.75	18.34	38
T19	300	0.5	0.5	-	-	-	-	-	-
T20	300	0.5	1	-617	45.66	60.25	-650.25	16.64	33.75
T21	300	0.5	1.5	-453.75	35.26	58	-459	23.71	28.75
T22	300	1	0.5	-648	52.63	63.25	-654.75	31.93	26.25
T23	300	1	1	-341	40.21	53.75	-346.5	26.11	31
T24	300	1	1.5	-314.25	11.18	52.5	-358	30.54	35.25
T25	300	1.5	0.5	-450.5	11.45	45.25	-476	32.30	28.25
T26	300	1.5	1	-311	19.24	48.5	-345.25	24.80	36
T27	300	1.5	1.5	-322	13.27	53.75	-328.75	28.62	36.75

P (MPa), f (m/min), STD (mm), σ(MPa)

On the other hand, the pressure has no impact on the residual stress state (**Fig. 17**) in both longitudinal and transverse directions. Nevertheless, residual stresses seem to decrease when increasing

traverse speed and step-over distance (**Fig. 17**). This may be due to the fact that the abrasive particles at higher speeds have less impact on the machine surface due to short exposure time.

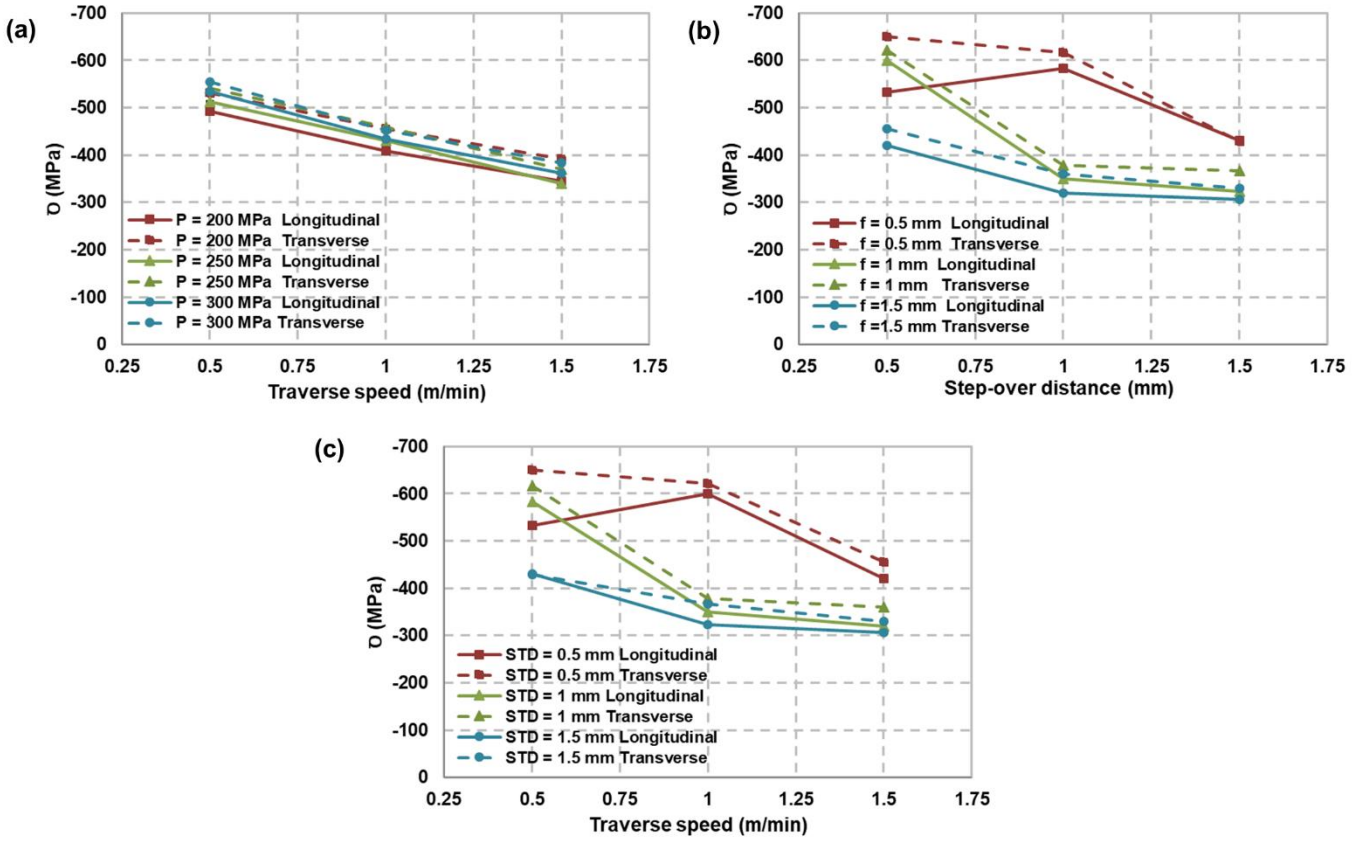

Fig. 17. Effect of traverse speed and step-over distance at constant pressure on residual stresses along longitudinal and transverse directions.

Based on the various results obtained in the study, in the **Table 6** the main characteristics of the machined surface when milling IN718 with AWJ is presented. These results indicate the range of surface integrity values and show the test numbers with which the minimum and maximum results values were obtained.

Table 6 AWJ milling results on different aspects of surface integrity of IN718

Surface integrity	**Surface roughness, Sa (μm)**	**Pocket depth, h (mm)**	**Material removal rate, MRR (mm^3/s)**	**Residual stress (MPa)**	
				σ_{xx}	σ_{yy}
	12.23 – 24.58	0.26 – 2.53	9.73 – 15.86	-292 to -648	-298 to -655
Minimal	T4	T9	T8	T18	T18
Maximal	T20	T1	T20	T22	T22

The evaluation of the effects on surface integrity aspects after AWJ milling in IN718 is also summarized in **Table 7**.

Table 7 Effect of AWJ milling parameters on different aspects of surface integrity of IN718

Machining parameters	Surface roughness	Pocket depth	Material removal rate	Residual stress
$P\uparrow$	↑	↑	↑	≈
$f\uparrow$	↓	↓	↓	↓
$STD\uparrow$	↕	↓	≈	↓
$P\uparrow + f\uparrow$	↑	↑		↑
$P\uparrow + STD\uparrow$	↑			
$P\uparrow + STD\downarrow$			↑	
$f\downarrow + STD\downarrow$		↑		↑

↑ increase, ↓ decrease, ↕ no clear effect, ≈ almost constant

4 Conclusions

In this study, the influence of the AWJ milling parameters $viz.$ jet pressure, traverse speed and step-over distance on surface roughness, topography, pocket depth and residual stress when milling Inconel 718 by AWJ were investigated experimentally. The following conclusions can be drawn from the study:

- The surface roughness (Sa) varies from $12.2\ \mu m$ to $24.6\ \mu m$. Surface roughness increases with the increase in pressure but decreases with increasing traverse speed. In addition, the milled surfaces presented a homogeneous texture with embedded abrasive particles. The jet pressure plays an important role in creation of crater defects. The crater size and depth increase with increasing jet pressure.
- The pocket depths vary between $0.26\ mm$ and $2.53\ mm$. An increase in pressure leads to an increase in pocket depth, but a decrease was observed when increasing traverse speed and step-over distance.
- A model to predict the pocket depth in function of machining parameters was obtained and was experimentally validated. The model can predict the pocket depth with 96% of accuracy and a maximum deviation of 5 % between the measured and predicted values.
- AWJ machining produces a high compressive residual stress state for all milled surfaces, which values are very close in both longitudinal and transverse directions (from $-292\ MPa$ to $-655\ MPa$), which indicate no effect on residual stress due to the tool path. In addition, the pressure parameter has no effect on residual stresses and the increase of the traverse speed and step-over distance favors the reduction in residual stresses.

- AWJ is a promising process to be used instead of conventional methods for milling IN718, nevertheless, after AWJ machining, the surfaces need to be cleaned to remove embedded abrasive particles, which generates up to 300% more surface roughness than conventional process.

Acknowledgments

The authors gratefully acknowledge the financial support of CONACYT Mexico. The authors also thank S. Le Roux for assistance with surface topography.

5 References

[1] J. Campbell and C. Flake, Manufacturing technology for aerospace structural materials, Elsevier, 2011.

[2] A. Bunsch, J. Kowalska and M. Witkowska, "Influence of die forging parameters on the microstructure and phase composition of Inconel 718 alloy," *Archives of Metallurgy and Materials,* vol. 57, pp. 929-935, 2012.

[3] R. M'Saoubi, T. Larsson, J. Outeiro, Y. Guo, S. Suslov, C. Saldana and S. Chandrasekar, "Surface integrity analysis of machined Inconel 718 over multiple length scales," *CIRP annals,* vol. 61, pp. 99-102, 2012.

[4] J. Zhou, V. Bushlya, P. Avdovic and J. E. Stahl, "Study of surface quality in high speed turning of Inconel 718 with uncoated and coated CBN tools," *The International Journal of Advanced Manufacturing Technology,* vol. 25, pp. 141-151, 2012.

[5] A. Devillez, G. Le Coz, S. Dominiak and D. Dudzinski, "Dry machining of Inconel 718, workpiece surface integrity," *Journal of Materials Processing Technology,* pp. 1590-1598, 2011.

[6] J. Holmberg, J. Berglund, A. Wretland and T. Beno, "Evaluation of surface integrity after high energy machining with EDM, laser beam machining and abrasive water jet machining of alloy 718," *The International Journal of Advanced Manufacturing Technology,* vol. 100, pp. 1575-1591, 2019.

[7] D. Umbrello, "Investigation of surface integrity in dry machining of Inconel 718," *The International Journal of Advanced Manufacturing Technology,* vol. 69, pp. 2183-2190, 2013.

[8] J. Zhou, V. Bushlya, R. Peng, S. Johansson, P. Avdovic and J. Stahl, "Effects of tool wear on subsurface deformation of nickel-based superalloy," *Procedia Engineering,* vol. 19, pp. 407-413, 2011.

[9] D. Aspinwall, R. Dewes, E.-G. Ng, C. Sage and S. Soo, "The influence of cutter orientation and workpiece angle on machinability when high-speed milling Inconel 718 under finishing conditions," *International Journal of Machine Tools and Manufacture,* vol. 47, pp. 1839-1846, 2007.

[10] M. Imran, P. T. Mativenga, A. Gholinia and P. J. Withers, "Evaluation of surface integrity in micro drilling process for nickel-based superalloy," *The International Journal of Advanced Manufacturing Technology,* 2011.

[11] U. Goutham, B. S. Hasu, G. Chakraverti and M. Kanthababu, "Experimental investigation of pocket milling on Inconel 825 using abrasive water jet machining," *International Journal of Current Engineering and Technology,* vol. 6, no. 1, pp. 295-302, 2016.

[12] A. Alberdi, A. Rivero, L. López de Lacalle, I. Etxeberria and A. Suárez, "Effect of process parameter on the kerf geometry in abrasive water jet milling," *The International Journal of Advanced Manufacturing Technology,* vol. 51, pp. 467-480, 2010.

[13] G. Fowler, I. Pashby and P. Shipway, "The effect of particle hardness and shape when abrasive water jet milling titanium alloy Ti6Al4V," *Wear,* vol. 266, pp. 613-620, 2009.

[14] T. Gupta, J. Ramkumar, P. Tandon and N. Vyas, "Role of process parameters on pocket milling with Abrasive Water Jet Machining technique," *International Journal of Mechanical and Mechatronics Engineering,* vol. 7, no. 10, pp. 348-353, 2013.

[15] A. Alberdi, A. Rivero and L. López de Lacalle, "Experimental study of the slot overlapping and tool path variation effect in abrasive waterjet milling," *Journal of Manufacturing Science and Engineering,* vol. 133, no. 3, pp. 034502-1, 2011.

[16] A. W. Momber and R. Kovacevic, Principles of Abrasive Water Jet Machining, Springer, 1998, p. 394.

[17] P. Hreha, A. Radvanská, S. Hloch, V. Perzel, G. Królczyk and K. Monková, "Determination of vibration frequency depending on abrasive mass flow rate during abrasive water jet cutting," *The International Journal of Advanced Manufacturing Technology,* 2015.

[18] P. Hreha, A. Radvanská, L. Knapcikova, G. Królczyk, S. Legutko, J. Królczyk, S. Hloch and P. Monka, "Roughness parameters calculation by means of on-line vibration monitoring emerging from AWJ interaction with material," *Metrology and Measurement Systems,* 2015.

[19] X. Sourd, R. Zitoune, A. Hejjaji, M. Salem, L. Crouzeix and D. Lamouche, "Multi-scale analysis of the generated damage when machining pockets of 3D woven composite for repair applications using abrasive water jet process: Contamination analysis," *Composites Part A: Applied Science and Manufacturing,* vol. 139, p. 106118, 2020.

[20] A. Hejjaji, R. Zitoune, L. Crouzeix, S. Le Roux and F. Collombet, "Surface and machining induced damage characterization of abrasive water jet milled carbon/epoxy composite specimens and their impact on tensile behavior," *Wear,* vol. 376, 2017.

[21] V. Bhandarkar, V. Singh and T. V. K. Gupta, "Experimental analysis and characterization of abrasive water jet machining of Inconel 718," *Materials Today: Proceedings,* 2019.

[22] A. Rivero, A. Alberdi, T. Artaza, L. Mendia and A. Lamikiz, "Surface properties and fatigue failure analysis of alloy 718 surfaces milled by abrasive and plain waterjet," *The International Journal of Advanced Manufacturing Technology,* vol. 94, no. 5-8, pp. 2929-2938, 2018.

[23] F. Cenac, R. Zitoune, F. Collombet and M. Deleris, "Abrasive water-jet milling of aeronautic aluminum 2024-T3," *Proceedings of the Institution of Mechanical Engineers, Part L: Journal of Materials: Design and Applications,* vol. 229, 2015.

[24] G. Escobar-Palafox, R. Gault and K. Ridgway, "Characterisation of abrasive water-jet process for pocket milling in Inconel 718," *Procedia CIRP,* vol. 1, pp. 404-408, 2012.

[25] M. Ay, U. Ç. and H. Ahmet, "Effect of traverse speed on abrasive waterjet machining of age hardened Inconel 718 nickel-based superalloy," *Materials and Manufacturing Processes,* vol. 25, no. 10, pp. 1160-1165, 2010.

[26] X. Sourd, R. Zitoune, L. Crouzeix, M. Salem and M. Charlas, "New model for the prediction of the machining depth during milling of 3D woven composite using abrasive waterjet process," *Composite Structures,* vol. 234, 2020.

[27] V. Bui, P. Gilles, T. Sultan, G. Cohen and W. R., "A new cutting depth model with rapid calibration in abrasive water jet machining of titanium alloy," *The International Journal of Advanced Manufacturing Technology,* 2017.

[28] X. Cai, S. Qin, J. Li, Q. An and M. Chen, "Experimental investigation on surface integrity of end milling nickel-based alloy Inconel 718," *Machining Science and Technology,* 2014.

Ethical Approval

This manuscript has not been submitted to, nor is under review at, another journal or other publishing venue neither in full nor part of it.

Consent to Publish

The authors give their consent for the publication of identifiable details, which can include photograph(s) and/or details within the text to be published in the above journal.

Authors Contributions

All authors have participated in (a) conception, experimentation, analysis and interpretation of the data; (b) drafting the article or revising it critically for important intellectual content; and (c) approval of the final version.

Competing Interests

The authors declare that they have no conflict of interest. The authors certify that they have no affiliations with or involvement in any organization or entity with any financial interest, or non-financial interest in the subject matter or materials discussed in this manuscript.

Availability of data and materials

The dataset generated in this research work is not shared at this point of time. However, the readers can approach the corresponding author if required.

Acknowledgements

This project was realized in Clément Ader Institute (Paul SabatierUniversity of Toulouse 3). The authors wish to thank Xavier Sourd and Sabine Le Roux from Clément Ader Institute for their technical support.

Funding

This research work was supported by the Mexican Agency of research and Technology (CONACYT).

Figures

Figure 1

Experimental setup for AWJ milling.

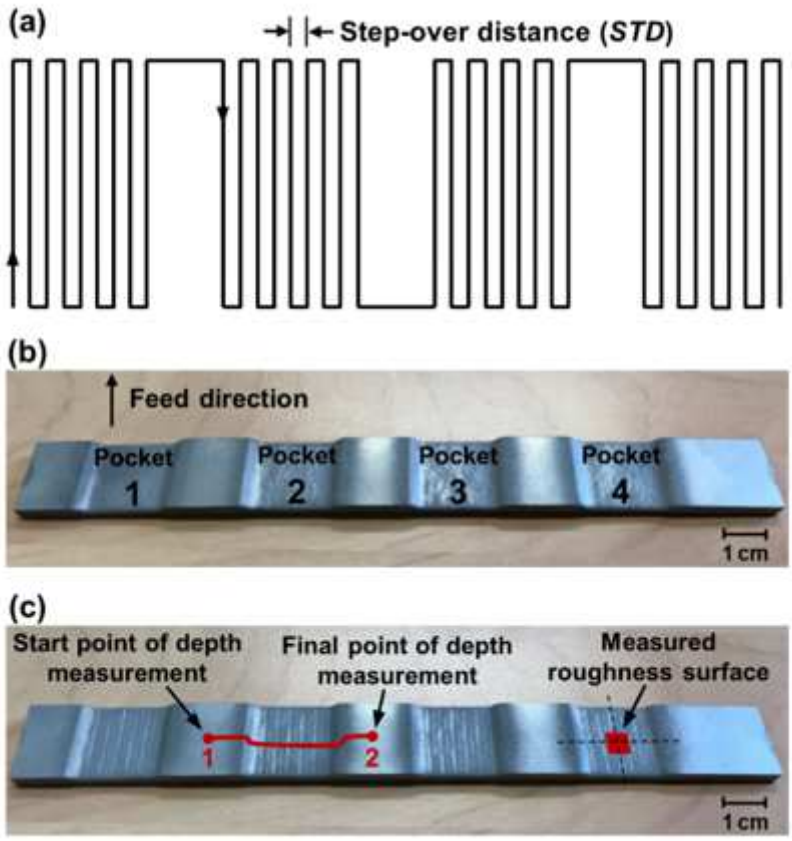

Figure 2

(a) Tool path; (b) Sample machined at P=250 MPa, f=1 m/min and STD=0.5 mm; (c) Location of pocket depth and roughness measurements of the pocket 2 and the pocket 4 respectively of the specimen milled at P=300 MPa, f=0.5 m/min and STD=1.5 mm.

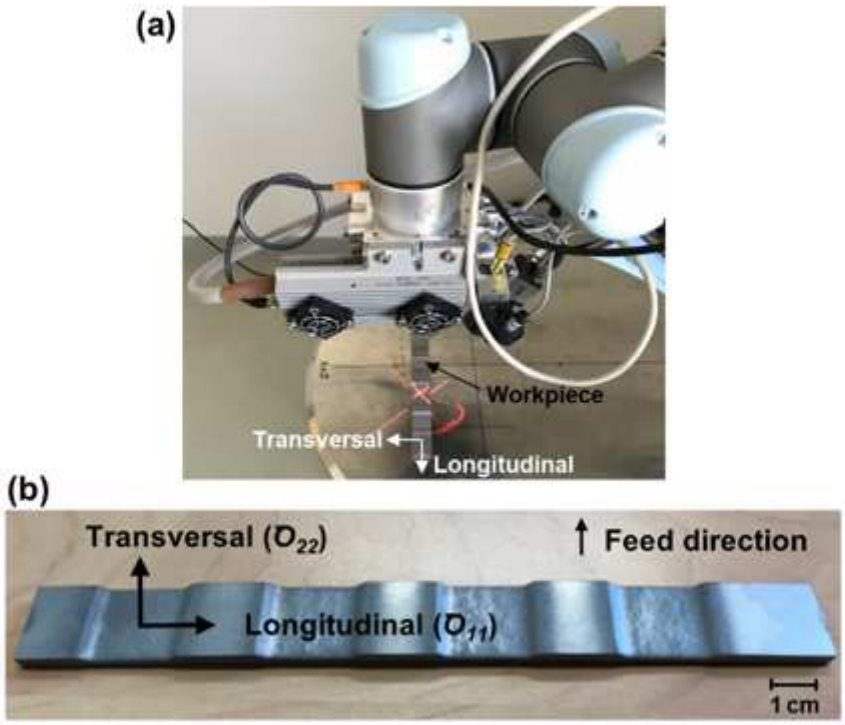

Figure 3

(a) Setup for the residual stress measurements; (b) Residual stress measurement directions.

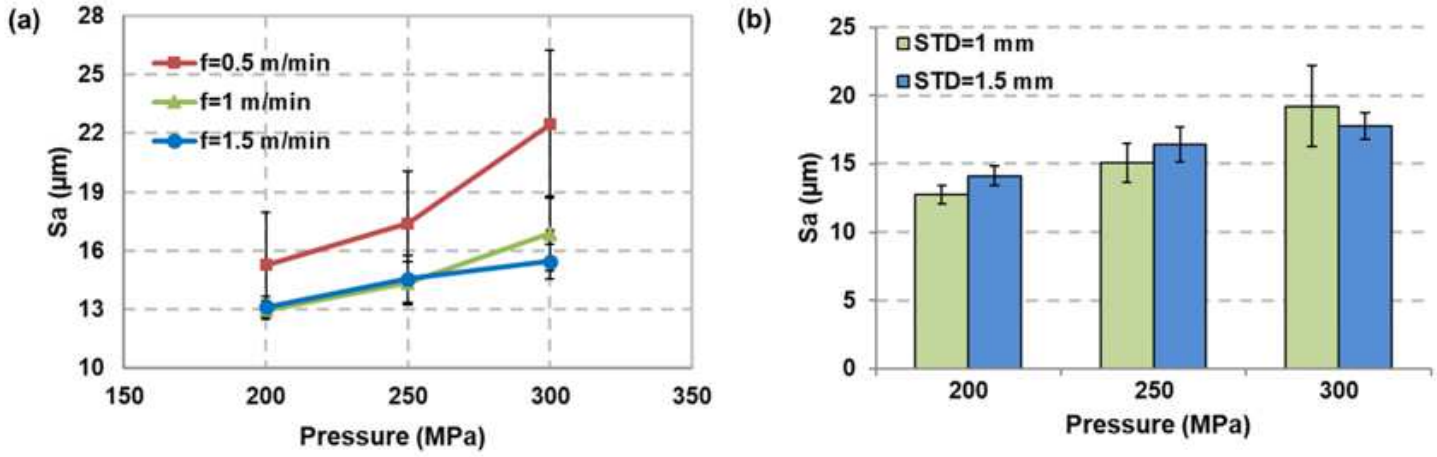

Figure 4

Effect of the pressure on surface roughness at (a) different traverse speed and (b) different step-over distance.

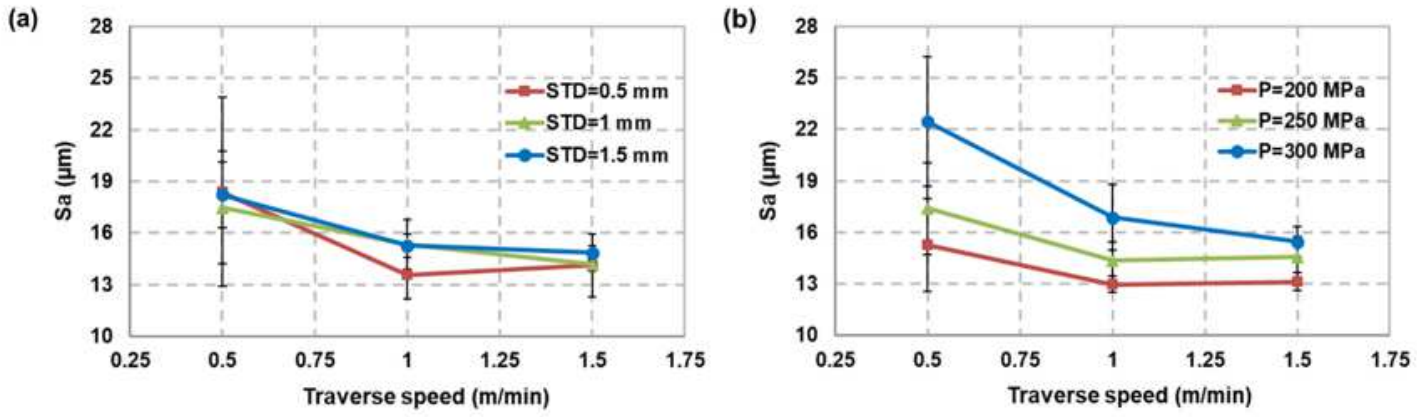

Figure 5

Mean effect of traverse speed on surface roughness at (a) different step-over distances and (b) at different water pressures.

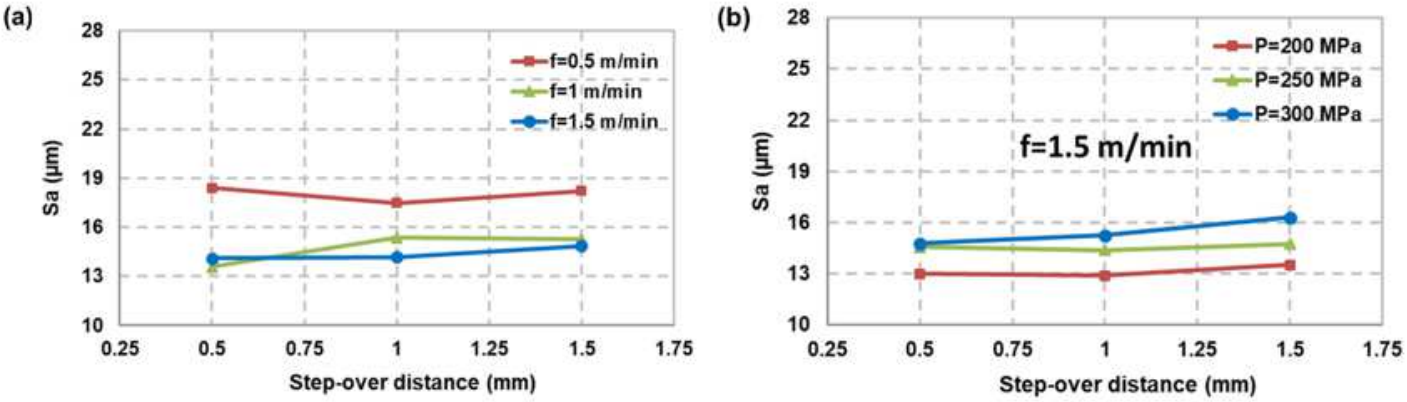

Figure 6

Effect of step-over distance on surface roughness (a) at different traverse speeds and (b) at different pressures with traverse speed of 1.5 m/min.

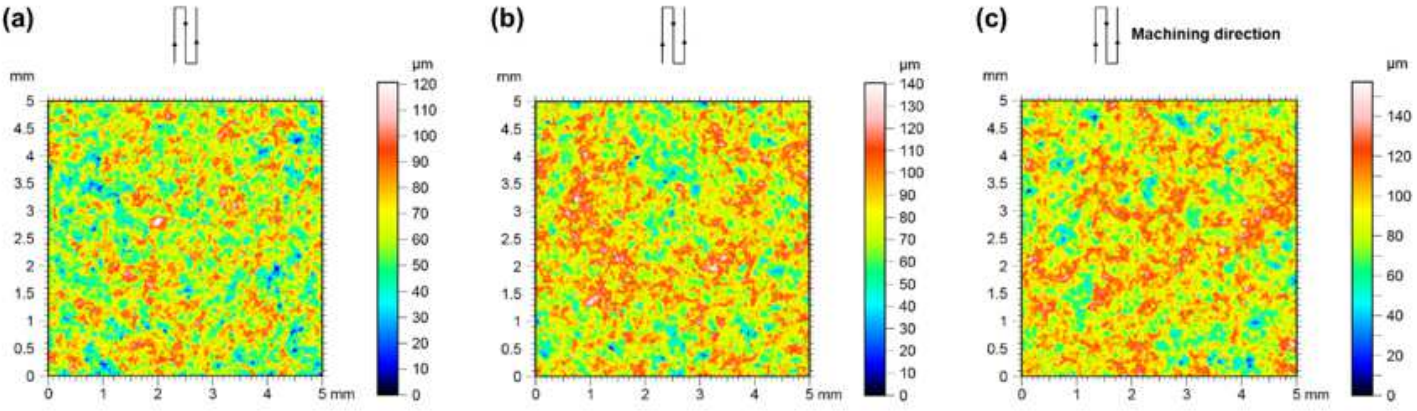

Figure 7

3D views of the milled surfaces by AWJ of samples machined at f=1.5 m/min, STD=1 mm and P of (a) 200 MPa, (b) 250 MPa, and (c) 300 MPa.

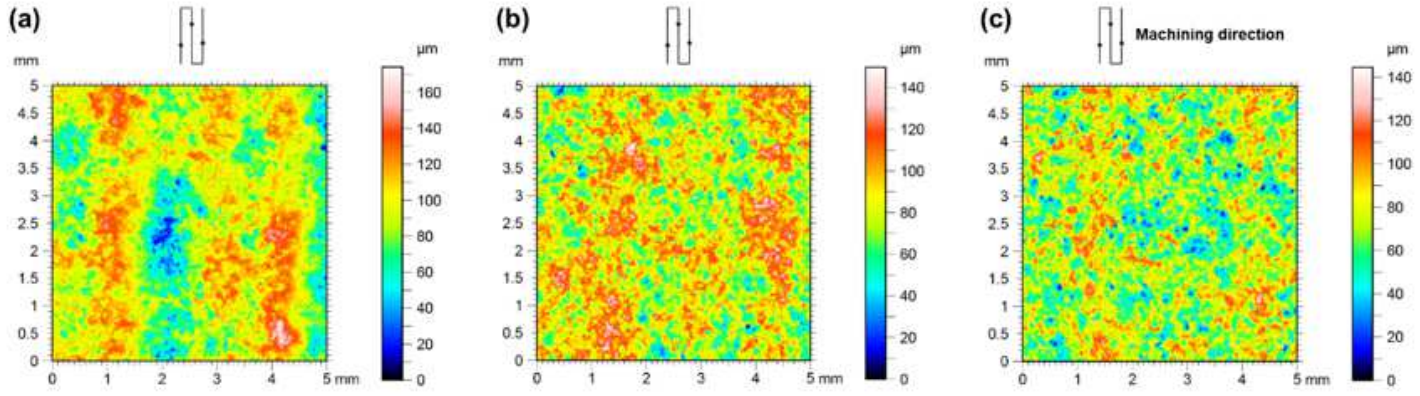

Figure 8

3D views of the milled surfaces by AWJ of samples machined at 250 MPa of pressure, STD=1.5 mm and (a) f=0.5 m/min; (b) f=1.0 m/min and (c) f=1.5 m/min.

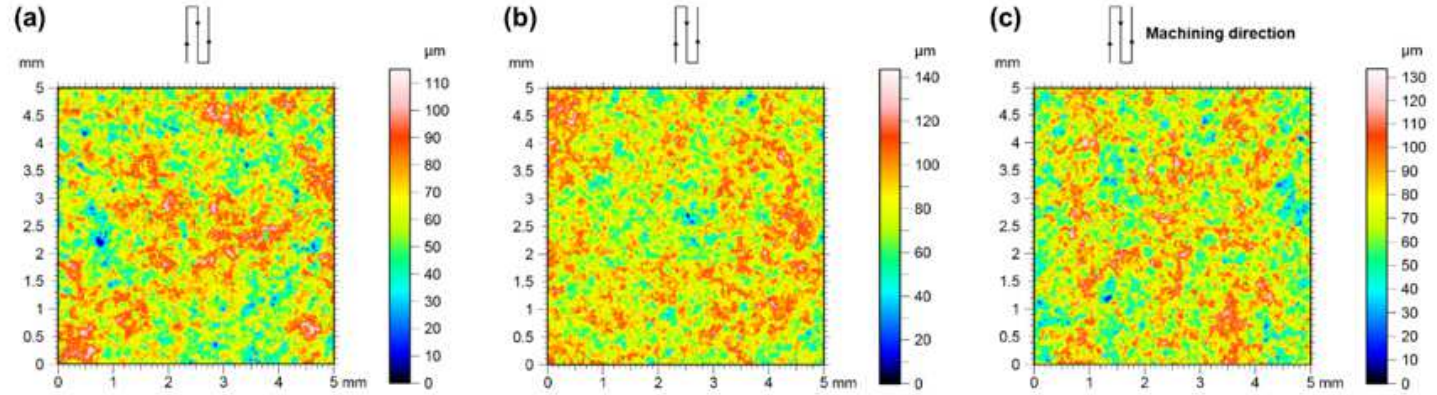

Figure 9

3D views of the milled surfaces by AWJ of samples machined at 200 MPa of pressure, f=1.5 m/min, P=200 MPa and (a) STD=0.5 mm; (b) STD=1 mm and (c) STD=1.5 m.

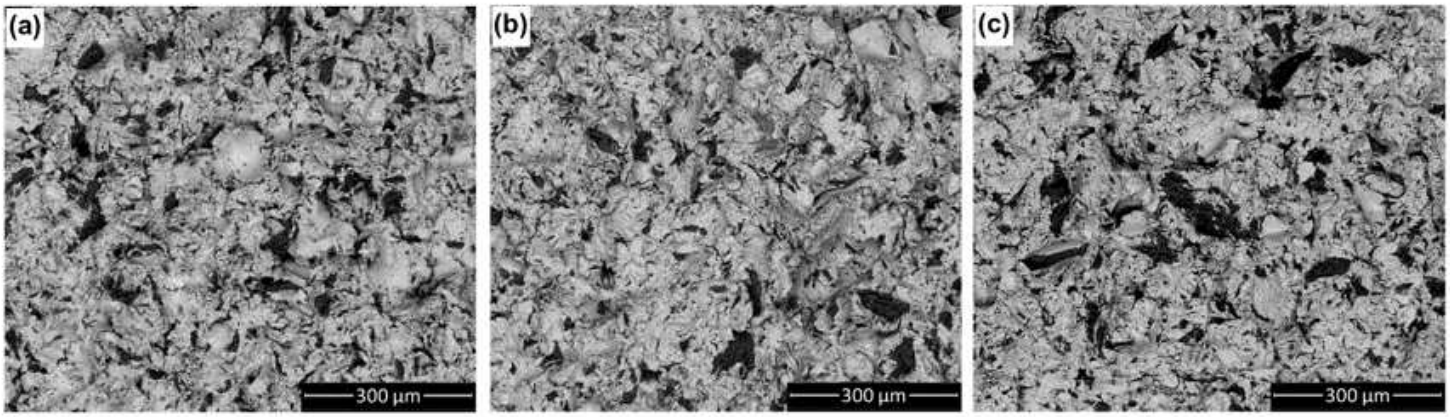

Figure 10

Micrographs from SEM in x 150 magnification of surfaces machined at f=1.5 m/min, STD=1 mm and P of (a) 200 MPa; (b) 250 MPa; and (c) 300 MPa.

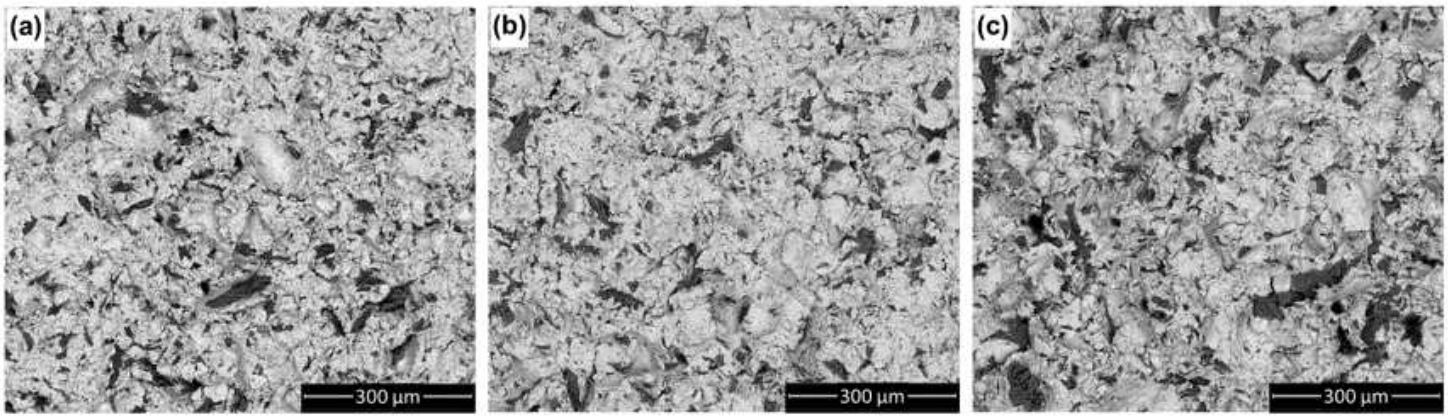

Figure 11

Micrographs from SEM in x 150 magnification of surfaces machined at 250 MPa of pressure, STD=1.5 mm and (a) f=0.5 m/min; (b) f=1.0 m/min; and (c) f=1.5 m/min.

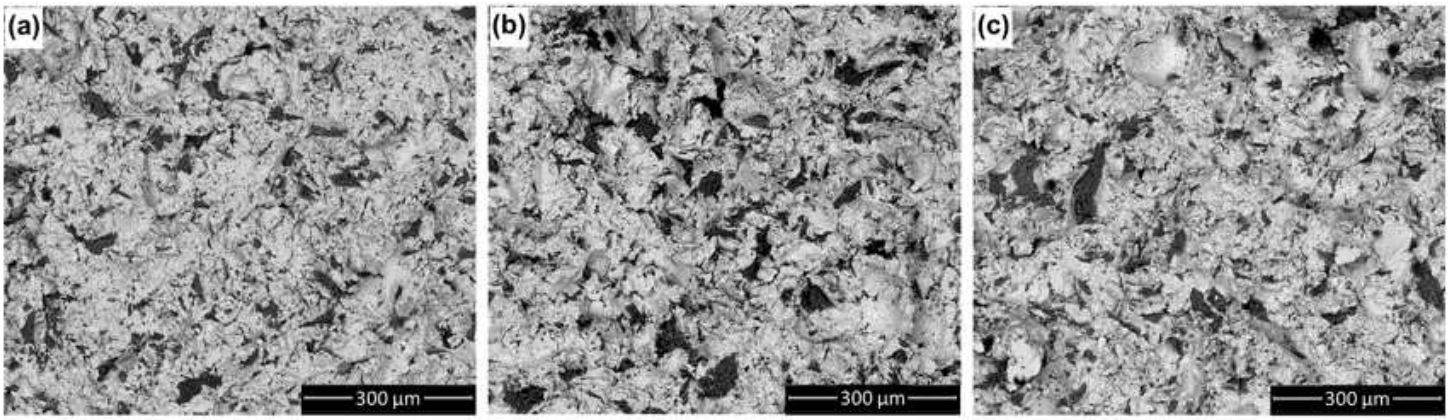

Figure 12

Micrographs from SEM in x 150 magnification of surfaces machined at 200 MPaof pressure, f=1.5 m/min and (a) STD=0.5 mm; (b) STD=1 mm; and (c) STD=1.5 m.

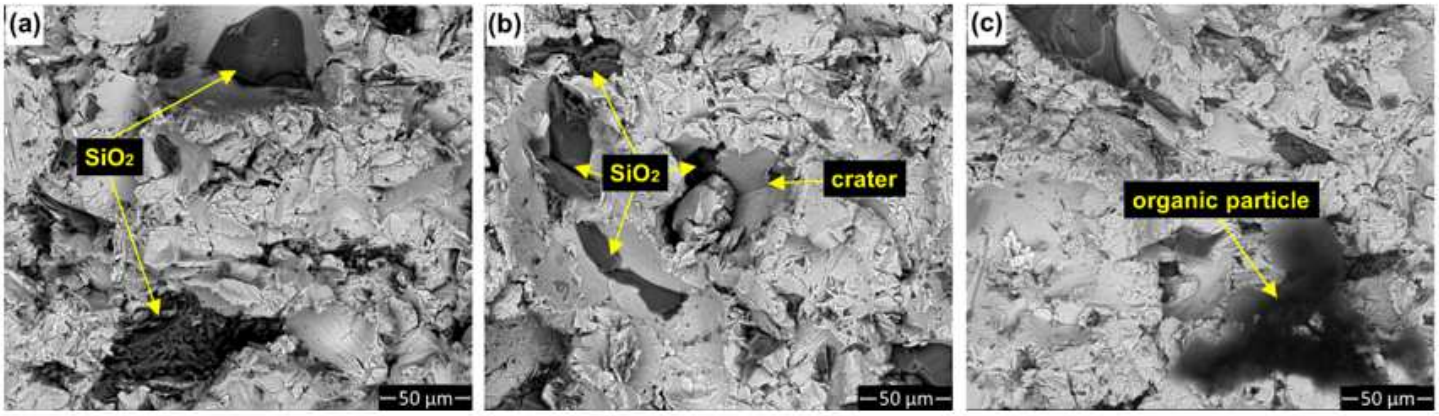

Figure 13

SEM images of different abrasive particles, (a) silica particles when machining at P=200 MPa, (b) abrasive particles and crater when machining at P=250 MPa , and (c) organic particle at when machining at P=200 MPa.

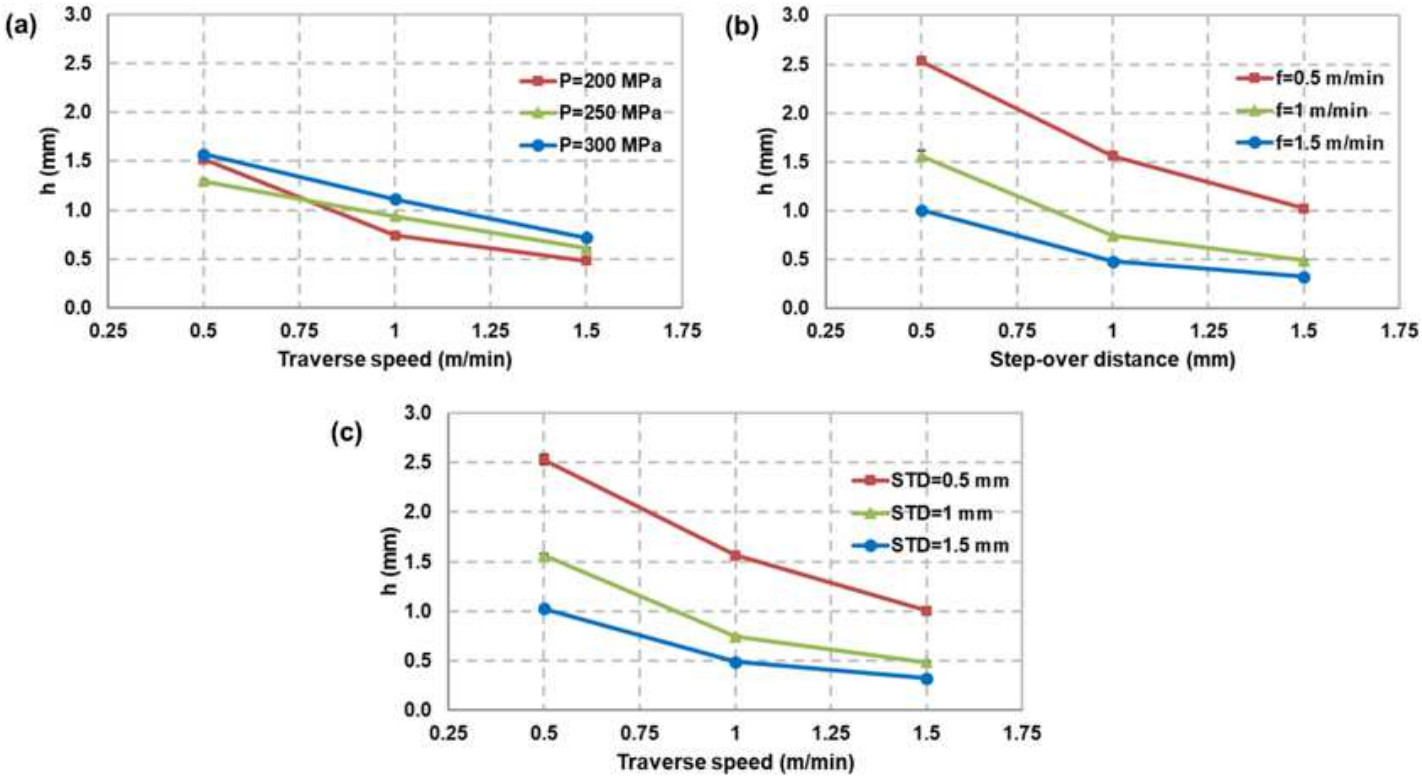

Figure 14

Effect of the (a) pressure, (b) traverse speed, and (c) step-over distance, on pocket depth.

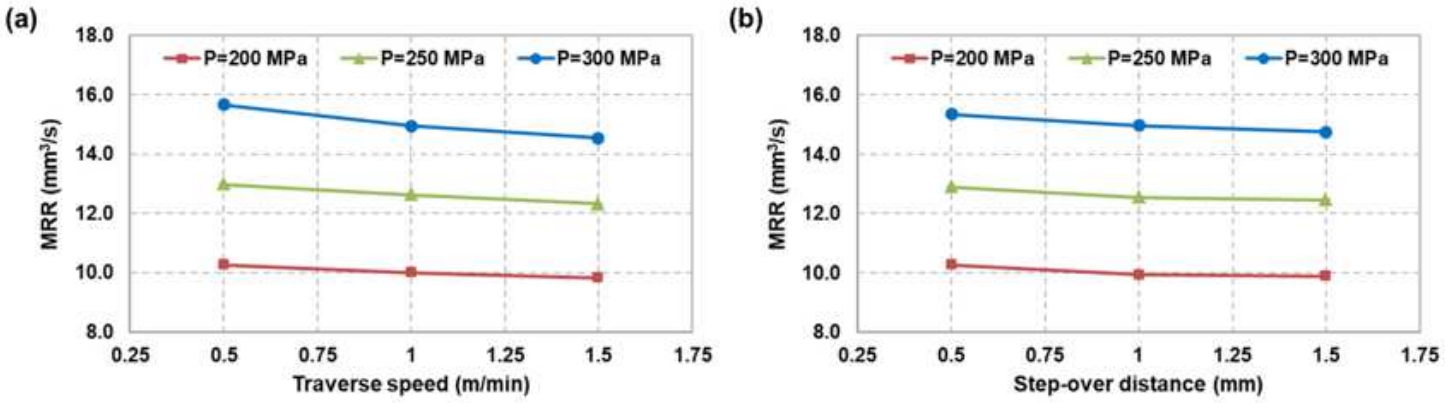

Figure 15

Effect of (a) the pressure and the traverse speed on the MRR, and (b) the pressure and the step-over distance on the MRR.

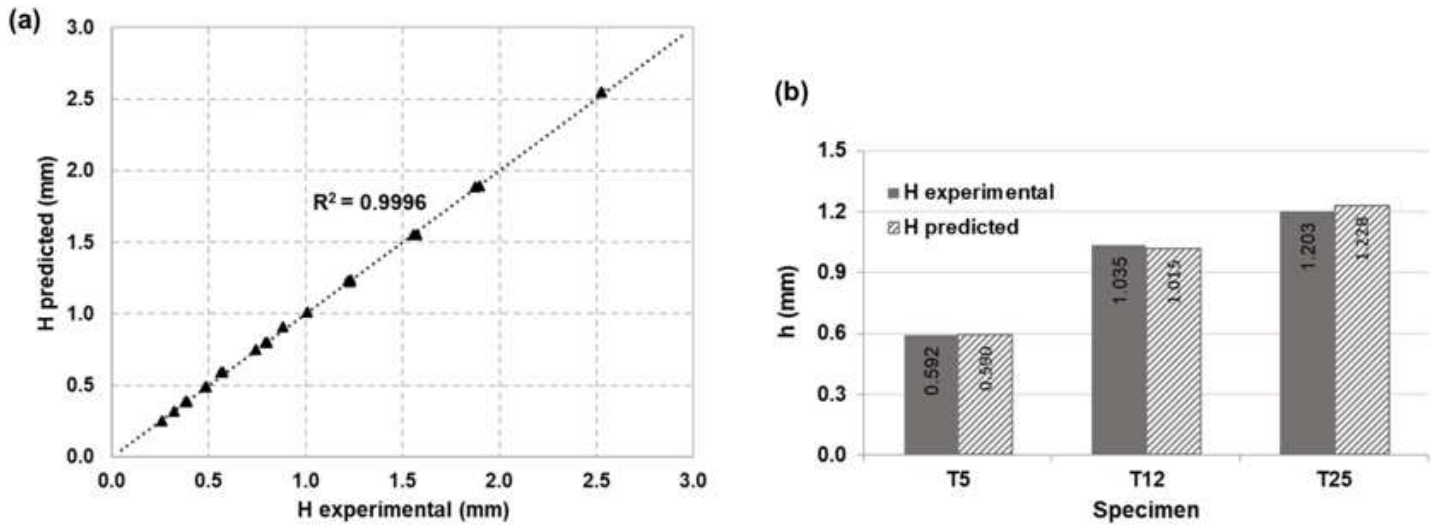

Figure 16

Graphs of the results of the predicted model, (a) experimental values in function of the predicted ones, and, (b) validation of the model.

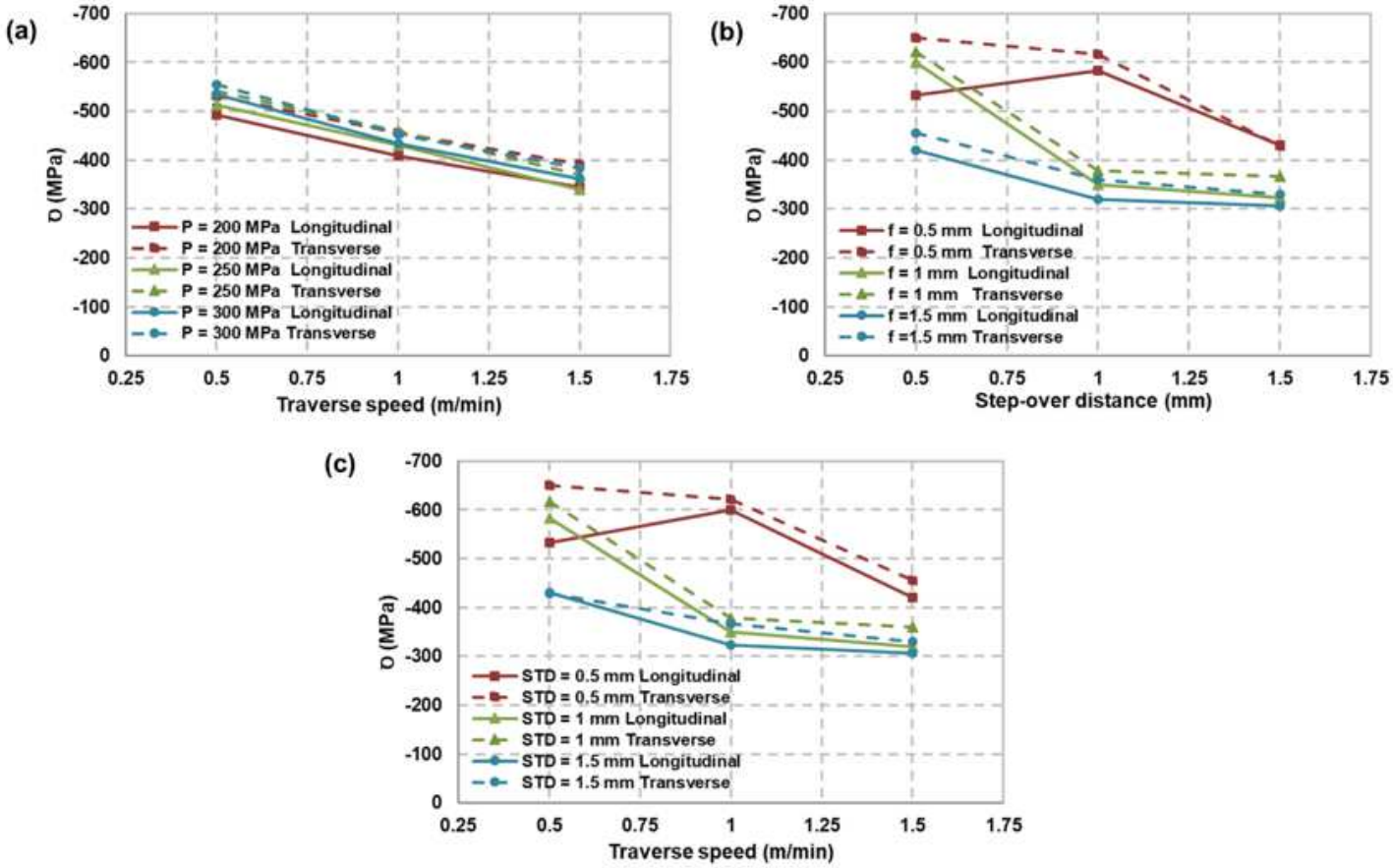

Figure 17

Effect of traverse speed and step-over distance at constant pressure on residual stresses along longitudinal and transverse directions.